2018

Investigation of Failure and Gassing in Advanced Lithium Ion Battery Systems with Electrolyte Optimization as a Solution

Jennifer Hoffmann
University of Rhode Island, j.hoffmann@gotion.com

INVESTIGATION OF FAILURE AND GASSING IN ADVANCED LITHIUM ION BATTERY SYSTEMS WITH ELECTROLYTE OPTIMIZATION AS A SOLUTION

BY

JENNIFER HOFFMANN

A DISSERTATION SUBMITTED IN PARTIAL FULFILLMENT OF THE REQUIREMENTS FOR THE DEGREE OF

DOCTOR OF PHILOSOPHY

IN

CHEMISTRY

UNIVERSITY OF RHODE ISLAND

2018

DOCTOR OF PHILOSOPHY DISSERTATION

OF

JENNIFER HOFFMANN

APPROVED:

Dissertation Committee:

Major Professor Brett L. Lucht

Arijit Bose

Sze Yang

Nasser H. Zawia
DEAN OF THE GRADUATE SCHOOL

UNIVERSITY OF RHODE ISLAND
2018

ABSTRACT

Stronger emphasis on sustainability has become a necessity amongst all industries, and the automotive industry is no exception. The push to move toward hybrid electric vehicles (HEVs) and electric vehicles (EVs) has resulted in a need for lithium ion batteries delivering higher power over a wide temperature range with improved safety over a long lifetime. To accomplish these requirements, advanced electrode materials such as the high nickel cathode material $LiNi_{0.8}Co_{0.1}Mn_{0.1}O_2$ (NCM811) or the anode material $Li_4Ti_5O_{12}$ (LTO) have been sought after. The high nickel cathode materials come with the desired high capacity suitable for the power needed for automobile applications but comes with safety and cycle life troubles. Looking at the other electrode LTO comes with long cycle life and improved safety compared to the widely used graphite anode but has gassing and capacity setbacks. The purpose of this work has two focuses, anode and cathode, with the common goal of using electrolyte optimization to resolve these advanced material problems. Electrochemical performance testing, gas chromatography, and electrolyte formulation investigation has been conducted to understand the mechanism of gas production with the LTO anode material. Results from this showed the gas evolution is directly related to the electrolyte interacting with the surface of the LTO. By creating a passivation film to protect the surface of the electrode from the electrolyte reactions through additive optimization and electrolyte formulation, we reduced the amount of gas produced by the material. Electrochemical impedance spectroscopy (EIS), X-ray photoelectron spectroscopy (XPS), and ATIR-IR spectroscopy were used to characterize the surface film. Using the same concept of electrolyte optimization,

additives such as tris(trimethylsilyl)phosphate (TMSP) and Ethoxy pentafluoro cyclotriphosphazene (PFPN) were shown to provide performance benefits to NCM811 cathode material through electrochemical measurements and EIS. Through the experiments conducted and results gathered, this work shows the ability to make the advanced materials, such as NCM811 and LTO, viable materials for successful commercialization in lithium ion batteries.

ACKNOWLEDGMENTS

I'd like to thank my advisor, Professor Brett Lucht, for his support, guidance, and patience over the past four years. I would also like to thank Dr. Jing Li and Dr. Martin Payne for encouraging and supporting me and my work. Thank you to my URI colleagues and my committee members for their constant support and flexibility. I also would like to thank my company, Gotion, for their support and confidence in me.

Finally, I would like to thank my parents and family, friends, and teachers that have always pushed me to be my best self and to creatively pursue my dreams.

Thank you.

PREFACE

This thesis was written using the manuscript format. Chapter 1 is an introduction to lithium ion batteries. Chapters 2-4 are pending publication manuscripts that include the investigation of the LTO gassing mechanism, the influence of additives on LTO, and the influence of additives on NCM811 cathode.

TABLE OF CONTENTS

ABSTRACT ii

ACKNOWLEDGMENTS iv

PREFACE v

TABLE OF CONTENTS vi

CHAPTER 1 1

INTRODUCTION 1

Background 1

Working Concept of Lithium Ion Batteries 2

Electrode: Cathode 2

Electrode: Anode 3

Electrolyte 4

Review of the Problem 5

References 6

CHAPTER 2 8

INVESTIGATION INTO THE GASSING MECHANISM OF Li4Ti5O12 FOR LITHIUM ION BATTERIES IN POUCH CELLS 8

Abstract 9

Introduction 10

Experimental 11

Results and Discussion 15

Conclusion 21

References…….24

Tables and Figures……...27

Figure 2.1……..27

Figure 2.2……..28

Figure 2.3……..29

Table 2.1..……..30

Table 2.2..……..31

Figure 2.4……..32

Figure 2.5……..33

Figure 2.6……..34

Figure 2.7……..35

CHAPTER 3 36

THE EFFECTS OF ELECTROLYTE ADDITIVES ON Li4Ti5O12 AND HOW THEY IMPACT GASSING..... 36

Abstract……..……..37

Introduction……..……...……..38

Experimental……..…39

Results and Discussion……..43

Conclusion……47

References……49

Figures……...52

Figure 3.1……..52

Figure 3.2……..53

Figure 3.3……..54

Figure 3.4……..55

Figure 3.5……..56

Figure 3.6……..57

Figure 3.7……..58

Figure 3.8……..59

Figure 3.9……..60

CHAPTER 4 61

THE EFFECTS OF TRIS(TRIMETHYLSILYL)PHOSPHATE AND PHOSPHAZENE ADDITIVES ON LiNi0.8Co0.1Mn0.1O2 DURING HIGH TEMPERATURE CYCLING 61

Abstract…….……62

Introduction……...63

Experimental…….64

Results and Discussion…….67

Conclusion……69

References……70

Figures……..73

Figure 4.1……..73

Figure 4.2……..74

Figure 4.3……..75

Figure 4.4……..76

Figure 4.5……..77

Figure 4.6…………………………………………………………………..78

Figure 4.7…………………………………………………………………..79

CHAPTER 1

INTRODUCTION

Background

Lithium ion batteries made their commercial debut when Sony released its battery based on $LiCoO_2$ (LCO), a carbon anode, and a non-aqueous electrolyte in 1991.[1] This momentous shift in energy storage and the battery industry was a result of researchers exploring the concepts of lithium intercalation for cathode materials[2], replacing pure lithium metal with lithium intercalated carbon as an anode material[3], and functional electrolytes that formed surface films and utilized non-aqueous, organic solvents[4]. Since its commercial debut, the increasing use in consumer goods has caused a demand in research to continue to deliver lithium ion batteries of higher energy and power. Paired with the political, industrial, and technological pushes toward sustainable means of energy and transportation, lithium ion batteries are the most competitive technology to deliver hybrid electric vehicles and electric vehicles due to their high capacity capabilities and long cycle life. To meet these demands, researchers have focused on developing new high capacity cathode materials, optimized battery management systems, advanced anode materials, and multi-functional electrolyte formulations.[1,5-7] With new materials being explored, come new issues that need to be solved including balancing safety, cost, and performance.

Working Concept of Lithium Ion Batteries

The working components of a lithium ion battery consist of a positive electrode (cathode), a negative electrode (anode), and the conductive, lithium ion transporting electrolyte. The two electrodes are separated from each other by a separator, which is most commonly made from a porous polymer membrane. The separator is inert in the system and serves as a means of preventing internal shorting of the cell. During charging, the positive lithium ions travel from the cathode (oxidation process) to the anode (reduction process). During discharge, the reverse happens, and lithium ions move back to the cathode from the anode. The electrolyte should be compatible with all components of the battery while reversibly shuttling the ions. Other components of the battery such as the battery management system (BMS), battery casing, and other engineering factors are also taken into consideration later in the development process.[8-9]

Electrodes: Cathode

At the birth of lithium ion batteries, the prominent cathode material was $LiCoO_2$ (LCO), which has a layered crystal structure. While this cathode material provides high theoretical specific capacity (274 mAh/g)[5] and strong cycling performance, the cost of cobalt and its low thermal stability leads to a material that proves to be expensive and unsafe. Other metals such as nickel and manganese were explored as replacement metals. Nickle provided high capacity and a lower cost but had cationic mixing and thermal stability issues on its own. Manganese was investigated for the reduced cost and provides improved safety, but the crystal lattice

shifts and the metal leaches out causing harm to the anode. LCO provides a rate performance advantage, nickel provides a capacity advantage, and the manganese provides a safety advantage. With all three metals offering different advantages with their own unique complications, the mixing of metals in the cathode material occurred to get a combination of the properties. More cobalt allows for better cycle and rate performance while more nickel allows for higher capacity. Increasing the manganese allows for thermal stability and overall safety in the material. Both nickel and manganese provide cost benefits.[1,5,10]

Electrodes: Anode

The carbon anode has been the commercially favored and most widely used anode material for more than 20 years.[5] Carbon anode operates at a low working potential versus lithium, is abundant and low cost, and shows the ability to have good cycle life if protected properly.[2,5,11] While suitable for consumer electronics, the demands of an electric vehicle have made it clear that new anode materials are attractive options. The anode material $Li_4Ti_5O_{12}$ (LTO) has been highlighted by many researchers as a viable candidate for these higher power applications. LTO has a theoretical capacity (175 mAh/g)[5,12] lower than the carbon anode (>300 mAh/g) and a lower work voltage window , however, it has no volumetric change in the crystal lattice structure, high rate capabilities, long cycle life, and improved safety over the carbon anode.[5,12] Combining LTO with advanced cathode materials does allow for an improvement on the voltage window. That leads to the true problem with the LTO anode, which is the strong gassing that occurs at the surface.[12-14]

Electrolyte

The electrolyte for a battery is a complicated system of salt, solvent, and additive components. The solvents most widely used today are linear and cyclic carbonates such as ethylene carbonate (EC), ethyl methyl carbonate (EMC), dimethyl carbonate (DMC), diethyl carbonate (DEC), and propylene carbonate (PC). The most widely used salt is lithium hexafluorophosphate ($LiPF_6$). The use of EC with a carbon anode is nearly mandatory as it is used to form a solid electrolyte interface (SEI) layer on the anode surface for surface protection. However, it has a high viscosity which requires it to be mixed with the linear solvents. A perfect electrolyte formulation will be stable over a wide temperature and electrochemical range, have a low viscosity, and good solubility. Additives are added to the solvent mixture as a means of also protecting the anode and cathode material from interacting negatively with the electrolyte through oxidative side reactions.[1,6]

Review of the Problem

The main obstacles that lithium ion batteries must overcome to successfully be adapted into the HEV and EV industry involves improved power, safety, lifetime, and cost over a wide temperature range.[1,6] To meet these standards, advanced cathode, anode, and electrolyte must be created. This thesis work confronts these challenges by looking into the gassing mechanism of the LTO anode, how electrolyte can improve this material through surface protection and solvent optimization, and how electrolyte can improve the performance of a sought after high performance cathode material through additive optimization.

References

1. Schipper, F.; Aurbach, D., A brief review: past, present and future of lithium ion batteries . *Russian Journal of Electrochemistry,* **2016,** *52* (12), 1095-1121.

2. Mizushima, K.; Jones, P.C.; Wiseman, P.J.; Goodenough, J.B., Li_xCoO_2 ($0<x<-1$): A new cathode material of batteries of high energy density. *Materials Research Bulletin,* **1980,** *15* (6), 783-789.

3. Basu, S.; Zeller, C. ; Flanders, P.J. ; Fuerst, C.D.; Johnson, W.D.; Fischer, J.E., Synthesis and properties of lithium-graphite intercalation compounds. *Materials Science and Engineering,* **1979,** *38* (3), 275-283.

4. Fong, R.; Vonsacken, U. ; Dahn, J.R. ; Studies of lithium intercalation into carbon anodes using nonaqueous electrochemical-cells. *Journal of the Electrochemical Society,* **1990,** *137* (7), 2009-2013.

5. Nitta, N.; Wu, F.; Lee, J.T.; Yushin, G., Li-ion battery materials: present and future. *Materials Today,* **2015,** *18* (5), 252-264.

6. Etacheri, V.; Marom, R.; Elazari, R., Salitra, G., Aurbach, D., Challenges in the development of advanced Li-ion batteries: a review. *Energy Environmental Science* **2011,** *4*, 3243-3262.

7. Banerjee, A.; Shilina, Y.; Ziv, B.; Ziegelbauer, J.M.; Luski, S.; Aurbach, D., Halalay, I.C., Review - Multifunctional materials for enhanced Li-ion batteries durability: a brief review of practical options. *Journal of the Electrochemical Society* **2017,** *164* (1), A6315-A6323.

8. Deng, D., Li-ion batteries: basics, progress, and challenges. *Energy Science and Engineering* **2015,** *3*, 385-418.

9. Scrosati, B.; Abraham, K.M.; Van Schalkwijk, W.; Hassoun J., Lithium Batteries: Advanced Technologies and Applications. **2013.**

10. Schipper, F.; Erickson, E.M.; Christoph, E.; Shin, J.Y.; Chesneau, F.F.; Aurbach, D., Recent Advances and Remaining Challenges for Lithium Ion Battery Cathodes. *Journal of the Electrochemical Society* **2017,** *164* (1), A6220-A6228.

11. Tran, T.D.; Feikert, J.H.; Pekala, R.W.; Kinoshita, K.; Rate effect on lithium-ion graphite electrode performance. *Journal of Applied Electrochemistry* **1996,** *11*, 1161-1167.

12. Xu, G.; Han, P. ; Dong, S.; Liu, H.; Cui, G.; Chen, L., $Li_4Ti_5O_{12}$ based energy conversion and storage systems: status and prospects. *Coordination Chemistry Reviews* **2017,** *343*, 139-184.

13. Han, C.; He, Y.B.; Liu, M., Li, B., Yang, Q.H.; Wong, C.P., Wang, F., A review of gassing behavior in $Li_4Ti_5O_{12}$ based lithium ion batteries. *Journal of Materials Chemistry A* **2017,** *5, 6368-6381*.

14. Belharouak, I.; Koenig, G.M.; Tan, T.; Yumoto, H.; Ota, N.; Amine, K., Performance degradation and gassing of $Li_4Ti_5O_{12}/LiMn_2O_4$ lithium ion cells. *Journal of the Electrochemical Society* **2012,** *159* (8), A1165-A1170.

CHAPTER 2

INVESTIGATION INTO THE GASSING MECHANISM OF Li4Ti5O12 FOR LITHIUM ION BATTERIES IN POUCH CELLS

By

Jennifer Hoffmann[1,3]; Mickdy Milien[2]; Martin Payne[3]; Brett Lucht[4]

Manuscript Pending Publication in Journal of Electrochemistry

[1]PhD candidate, Department of Chemistry, The University of Rhode Island, Kingston, RI 02882.

[2]PhD graduate, Department of Chemistry, The University of Rhode Island, Kingston, RI 02882.

[3]Battery R&D, Gotion Inc., Independence, Ohio 44131, USA

[4]Professor, Department of Chemistry, The University of Rhode Island, Kingston, RI, 02882.

Abstract

Lithium titanate (LTO) has been looked at as one of the leading anode materials for lithium ion battery applications in grid storage and automotive applications. However, the material's main challenge is a gassing problem that causes the theoretically long lifetime of the cell to face early cell death. The causes of this gassing mechanism have been attributed to water impurities from the electrolyte, moisture trapped in the electrode, the breakdown of lithium salt forming hydrofluoric acid (HF), and/or solvent interactions with the surface of the electrode. The purpose of this work was to investigate the root cause of the gas formed during formation, high temperature storage, and high temperature cycling. In doing so, the effects of LiTFSI, LiFSI, EC free formulations, and a gas reducing additive (tris (trimethysilyl) borate) was presented. Using the EC free formulation and the gas reducing additive, we were able to successful reduce the amount of gas formed and confirm the gas produced by LTO is the result of electrolyte interactions rather than moisture or HF attacks.

Introduction

Lithium-ion batteries have garnered a lot attention due to their beneficial properties in electric and hybrid electric vehicles as well as in energy storage. While lithium titanate ($Li_4Ti_5O_{12}$, LTO) has a lower theoretical capacity of 175 mAh g^{-1} compared to carbon (372 mAh g^{-1}), it is an attractive anode material for these applications due to its long cycle life performance, 1.55V working potential which provides safety benefits, and zero volumetric lattice variation during charging and discharging [1-4]. Despite being regarded as one of the leading anode materials [5], it suffers from large gas evolution at elevated temperatures causing premature cell life termination [6-8].

Many investigations into this gas production by LTO has been conducted by different researchers throughout the field. One theory that has been researched in the influence of water contamination from humidity, electrolyte contamination, and/or trapped hydroxyl groups on the surface of the LTO during production [7,9,10]. Other research as investigated the lithium salt influence as the most common salt, lithium hexafluorophosphate ($LiPF_6$) is known to decompose at elevated temperatures to form hydrofluoric acid (HF) [12-14], which would be increased if there is water present in the LTO system. While the influence of water is understood to be detrimental to most lithium ion battery systems, recent work has been focusing on another potential cause of LTO gassing; interfacial reactions between the LTO surface and the electrolyte solvents [7-9,15-16]. This recent work has shown evidence that the source of majority of gas formed from LTO is from the solvents interacting with the different transition

states of the Ti on the outermost layer of the LTO surface. These surface reactions are reported to lead to decarboxylation, decarboxylation, and dehydrogenation of the electrolyte solvents [15]. While many researchers have investigated these findings either in pouch cells at room temperature or in other non-full cell formats at high temperature, we believe is the next step in LTO testing is to investigate in full cell pouch cells at elevated temperatures to create realistic battery scenarios. Therefore, electrolyte formulations replacing the $LiPF_6$ salt with imide salts, introducing an acid scavenging additive, testing an EC free formulation, and trying a novel LTO SEI additive were utilized to investigate some of the details of the gassing mechanism in LTO full cell, pouch cells at high temperature.

Experimental

Materials

The cathode active material was commercially available BTBM lithium manganese oxide (LMO) and the anode was commercially available POSCO $Li_4Ti_5O_{12}$ (LTO). The 920 mAh dry cell, multilayer pouch cells (MLPC) were assembled by SKC. Battery grade ethylene carbonate (EC), propylene carbonate (PC), diethyl carbonate (DEC), lithium hexafluorophosphate ($LiPF_6$), lithium bis(trifluoromethanesulfonyl)imide (LiTFSI), and lithium bis(fluorosulfonyl)imide (LiFSI) were obtained from BASF and used as received. Electrolyte additives dimethylacetamide (DMAc) and tris (trimethylsilyl) borate (TMSB) were obtained from Sigma Aldrich and used as received.

Electrolyte HF Storage Testing

To verify that the additives react with the electrolyte in the way that the experiment intended them to do, electrolyte underwent storage testing. Each formulation was made in a large batch and allocated in a nitrogen glove box into small aluminum, air tight bottles. Enough samples from each batch were stored to allow for three duplicates for each week measurement to ensure reproducibility. The first sample was tested after blending and right before the other bottles were added to storage.

The HF was measured using a Metrohm titrator with Tiamo software and a Metrohm double platinum wire 6.0341.100 pH electrode. In a Teflon beaker, about 50 grams of crush ice formed from deionized (DI) water and 50 grams and 60 grams of DI water is added. Cold water and ice is used to stall the formation of excess hydrofluoric acid (HF) formation from $LiPF_6$ reacting with moisture leading to false high readings. The beaker is set on the Metrohm titrator propeller stirrer and base, and the electrode is submerged. After the run is set, 5-10 mL of electrolyte is added to the beaker and the sample is titrated to equilibrium with 0.01N NaOH.

Pouch Cell Preparation

Dry cells were dried at 55°C for 12 hours under vacuum prior to filling. Cells were then filled with 9.1 grams of electrolyte and vacuum sealed in an argon dry box. To ensure proper wetting, the cells rested for 12 hours in a 25°C chamber, unclamped before starting formation and testing. Volume measurements were taken before formation.

Electrochemical Testing

Pouch cells were clamped and cycled with a constant current charge at 0.1C rate up to 2.8V using a MACCOR battery cycler. Upon complete charge, the cells were removed from the clamps and placed into a 45°C chamber for 12 hours for aging. Cells are then degassed and vacuum sealed in the argon dry box before re-clamping and undergoing second formation. Cells undergoing second formation were cycled with a constant current-constant voltage charge and constant current discharge between 2.8V and 1.7V with the following procedure: first cycle C/10, D/10, second cycle C/5, D/5, and third cycle 1C, 1D. After this second formation step, cycling and high temperature storage cells have separate procedures.

Cells that underwent high temperature storage (HTS) underwent the following before storage procedure with tight clamping: CCCV charge to 2.8V at 0.7C with a cutoff current of 0.02C, CC discharge to 1.7V at 1C, and CCCV charge to 2.8V at 0.7C with a cutoff current to 0.02C. In the 100% state of charge (SOC) the cells will undergo any other measurements that need to be taken and then stored under light clamping in a 60°C chamber for 7 days. At the end of the storage time, the cells will be removed from high temperature and undergo any room temperature measurements that are needed. The final step is the following after storage procedure under tight clamping: CC discharge to 1.7V at 1C, CCCV to 2.8V at 1C with a cutoff current of 0.02C, and CC discharge to 1.7V at 1C.

Cells that underwent cycling followed the second formation step with a rate test procedure that cycled between 2.8V and 1.7V with the following cycles: first and

second cycles C/2, D/2, third cycle C/2, D/5, fourth cycle C/2, D/2, fifth cycle C/2, 1D, sixth cycle C/2, 2D, and cycles seven through nine C/2, D/2. After rate test cells underwent a second aging step by undergoing the before storage procedure described previously. Cells are then stored under light clamping at 100% SOC for 24 hours. Cells then undergo the after-storage program described previously. Cells undergo any before high temperature cycling measurements and are placed into the 60°C chamber under tight clamping. The cells are cycled between 2.8V and 1.7V at 1C/1D with a C/10, D/10 cycle every 50^{th} cycle. Every 300 cycles the cells are suspended in the discharged state for volume measurement at room temperature. After volume measurement, cells then resume the same cycling procedure for another 300 cycles.

All cells were prepared in minimum of two duplicates to confirm reproducibility for all tests conducted.

Gas Analysis

Gas volume was measured before first formation, before aging after first formation, after aging before degassing, before storage and/or cycling, and after storage and/or cycling according to the procedure first described by Aiken et al. The pouch cells were hung from the bottom of scale and tarred. After reaching a stable zero, the cells were submerged completely to a defined level in 25°C deionized water. The recorded weight of the cell while submersed was then used along with the Archimedes' principle to calculate the amount of gas evolved over time [17].

To measure the composition of gasses, cells were brought into the argon dry box for extraction. A 0.5 mL Vici precision sampling analytical pressure-lok syringe

was used to manually extract the gas sample from the cell under argon atmosphere. The sample was then manually injected into a Varian 450 gas chromatograph equipped with a 19808 ShinCarbon ST column, thermal conductivity detector (TCD), and an argon carrier gas.

Results and Discussion

Electrolyte HF Storage Testing

Formulations were selected for storage testing to verify the acid scavenging additives chosen for this test were removing the acid from the electrolyte. The baseline electrolyte consists of 1.0 M $LiPF_6$ in EC/PC/DEC (15/20/65, v). Known acid scavenging additives DMAc and acid inhibitors such as LiTFSI were selected and added to the baseline at 0.25% and 1% respectively. The combination of these two additives was also tested. The final formulation tested removed all $LiPF_6$ from the formulation and replaced it with LiTFSI to show the contribution of HF from the lithium salt versus HF impurities in the electrolyte.

The results from each week are shown in Figure 2.1 with the amount of HF in ppm plotted as a function of time (week intervals). The fresh, initial levels of HF show that the $LiPF_6$ free formulation has no HF present indicating the battery grade solvents used do not have impurities and the main source of HF is from the $LiPF_6$ salt. The baseline formulation started with 25.224 ppm HF concentration. Both formulations with 0.25% DMAc also so no initial HF present indicating the DMAc successfully scavenged the HF initially present in the baseline due to $LiPF_6$ decomposition. The formulation with 1% LiTFSI showed a decrease in HF content compared to the

baseline but did not inhibit the HF formation entirely. The DMAc additive formulations showed HF formation inhibition for up to two weeks. At this time, we believe the additive was consumed and was no longer present to continue scavenging the HF formed from $LiPF_6$ decomposition. Interestingly, a synergistic effect is seen when combining LiTFSI and DMAc allowing for an extra week of storage without HF being present. The formulation with no $LiPF_6$ present did not show any HF formation during the entire four-week storage period indicating that the impurities in the electrolyte is not of concern with the battery grade materials obtained. The storage testing conducted in cells involved 60°C storage for 1 week indicating that 0.25% DMAc would be able to scavenge the acid formed during this amount of storage time.

High Temperature Storage Testing

Cells were filled with electrolyte formulations developed to test the hypothesized triggers for gas formation in LTO cells. The baseline and baseline with 0.25% DMAc are the same formulations used in the electrolyte storage test. The DMAc formulation was chosen to represent the acid scavenging condition to ensure any HF present from $LiPF_6$ breakdown, electrolyte impurity, or residual water from the LTO was removed during testing. Formulation Base 2S consists of 1.0 M LiTFSI in EC/PC/DEC (15/20/65, v) + 5% $LiPF_6$ while Base 2FSI consists of 1.0 M LiFSI in EC/PC/DEC (15/20/65, v) + 5% $LiPF_6$. These formulations were designed as an $LiPF_6$ replacement formulations to remove the influence of $LiPF_6$ salt on the system. These formulations contain additive levels of $LiPF_6$ to help combat corrosion and conductivity issues that is typically present when using LiTFSI or LiFSI in high

quantities. Base P.De is designed as an EC free formulation consisting of 1.0 M $LiPF_6$ in PC/DEC (35/65, v). The final formulation is the baseline with $LiPF_6$ salt and 1% TMSB. This additive was selected due to the LTO SEI it forms and the performance benefits seen during formulation screening.

After formation, including the aging step, the cells underwent the gas volume measurement. Figure 2.2a shows the results of the measured formation gas in each cell. The baseline had 3.650 mL of gas evolved. The acid scavenging formulation with DMAc had 1.268 mL more gas evolved compared to the baseline. The LiFSI salt replacement formulation had 5.870 mL more formation gas evolution than the baseline. The formulation with TMSB, EC Free, and LiTFSI salt replacement successfully reduced formation gasses with the LTO SEI forming TMSB additive having the lowest amount of formation gases.

The composition of formation gas for each formulation was investigated through GC-TCD as shown in Figure 2.3. The baseline formation gasses showed that 76.6% of the gas formed is hydrogen gas, which equated to 2.797 mL of hydrogen gas formed during formation as shown in Table 2.1. The remaining components of the baseline formation gases were composed of carbon monoxide (14.8%, 0.54 mL), carbon dioxide (4.9%, 0.178 mL), ethylene (2.6%, 0.095 mL), and methane (1.1%, 0.04 mL). Replacing the $LiPF_6$ salt with LiTFSI showed a larger percentage of the gas was hydrogen compared to the baseline, but with less net gas formed, it produced 0.14 mL less hydrogen than the baseline. The LiFSI salts showed the largest increase of hydrogen gas compared to the baseline both in terms of percentage of composition and in gas volume. The overall composition of the imide salt replacement formulations

matched the baseline composition indicating the change in salt did not display a large change to the formation gassing mechanism but may have influenced the rate of reaction. Removing the EC from the electrolyte showed a 0.374 mL increase in hydrogen gas formed despite decreasing the amount of net gas produced. The decreased amount of gas formed during formation is due to the absence of ethylene and carbon dioxide forming during formation; only hydrogen, carbon monoxide, and methane were present. While this data shows the EC was not the source of hydrogen gas during formation, this phenomenon provides initial evidence that the solvent choice plays a role in composition and quantity of the gas produced during formation. The acid scavenger showed a 9.47% or 1.44 mL increase in hydrogen gas than the baseline indicating removing the HF during the formation was not the source of initial hydrogen gas. The acid scavenger also showed no ethylene or carbon dioxide present. The formulation containing TMSB showed the lowest amount of gas formed, and despite the percentage of hydrogen gas being 14.1% greater than the baseline, it had 0.535 mL less hydrogen formed in addition to significantly reduced amounts of the carbon gases. This was the smallest amount of hydrogen gas and net gas produced during formation. Further investigation is needed to characterize the SEI, but the protecting layer shows evidence of electrolyte stabilization and reduced interaction with the surface of the LTO during formation.

After cells were removed from high temperature storage for one week, the volume and gas analysis were analyzed again. The gas measured and analyzed during this step is only from storage as the cells were degassed after the formation phase. Figure 2.2b shows the amount of gas evolved after the week of storage. The only

formulation that reduced the gas evolved after storage was the 1% TMSB formulation, which was 0.721 mL less than the baseline. This is evidence that protecting the LTO can be an effective means of reducing the gas in formation and for long term, high temperature performance. The formulation with DMAc and LiFSI salt replacement showed the largest amount of gas evolved after storage.

The gas composition after HTS showed new gases formed compared to the formation gas composition as seen in Figure 2.4. The baseline gas after HTS consisted of 70.62% hydrogen gas (4.864 mL) which is the largest component. In addition to the hydrogen gas, the baseline showed 14.31% carbon monoxide, 7.845% carbon dioxide and ethane, and 0.88% methane and ethylene. The presence of ethane was not initially seen during the formation gassing. Similar to the formation gas composition, the LiTFSI replacement formulation had a similar profile to the baseline but produced 0.81 mL more hydrogen and more ethane in the baseline as seen in Table 2.2. The LiFSI replacement showed a large difference in composition with a reduced portion of the gas being hydrogen, but with the large amount of gas formed it still produced 0.71 mL more hydrogen than the baseline. Both salt replacement formulations showed negative impact on net amount of gas produced as well as amount of hydrogen produced in the system. The EC free formulation had 0.86 mL more gas formed than the baseline with 1.141 mL more hydrogen formed. Noticeably present in the composition of EC free storage gas was propene, not seen in the other formulations, indicating the concentration of PC was likely too high and not a suitable high temperature substitute for EC. The second largest amount of gas formed during storage came from the DMAc formulation, which produced 3.432 mL more gas and

2.670 mL more hydrogen gas than the baseline. Similar to the formation gas trend, TMSB successfully reduced the amount of net gas formed after storage by 10.5% and reduced the amount of hydrogen gas by 4.95% or 0.232 mL despite the hydrogen gas making up a larger percentage of the TMSB gas formed than the baseline.

While reducing the gassing of the cells and understanding the mechanism causing the gassing in LTO systems is important, the cell performance was recorded to track the influence of each method in Figure 2.5. Replacing $LiPF_6$ with LiTFSI resulted in an improvement in the remaining and recovered capacity compared to the baseline, while using LiFSI performed the worst. The EC free formulation showed strong recovered capacity but showed reduced remaining capacity. Both DMAc and TMSB formulations had both recovered and remaining capacity greater than 85%.

High Temperature Cycling

High temperature cycling is conducted at 45°C compared to the 60°C that high temperature storage takes place. Figure 2.6 shows the capacity retention of the formulations investigated in the storage testing after 600 cycles. After 600 cycles, the EC free formulation has the best retention with 96.5% capacity retention. While the EC free formulation did show performance loss during storage, at 45°C the EC free is able to perform without the PC breakdown becoming harmful to the system. The other formulations did not outperform the baseline, but the LiFSI salt replacement formulation and 0.25% DMAc formulations performed the worst with Base 2FSI showing fast capacity fade after 200 cycles and only 87.1% capacity retention after 600 cycles. Base with DMac showed 92% capacity retention after 600 cycles. Base 2S

and Base with TMSB both showed about 93.4% capacity retention after 600 cycles.

During high temperature cycling, the amount of volume of gas each cell produced was measured after every 300 cycles. The volume measurement was conducted at 25°C after the cells were rested to stabilize temperature, and the gas produced is shown in figure 2.7. After 300 cycles, the TMSB and EC free formulations both reduced the amount of gas formed by 4.26% and 2.23% respectively. Following the same trend as formation and storage gassing, Base 2FSI and base with DMAc showed the largest amount of swelling with the acid scavenger formulation producing 10.66 mL of gas; more than double the baseline. After 600 cycles, the EC free and TMSB had reduced the amount of gas by more than 17.8%. The DMAc formulation had produced so much gas, that the cells floated during measurement and an accurate value could not be obtained. Composition of the gas formed was conducted after 300 cycles for the baseline, but other composition testing is ongoing. Initial results showed similar composition to the high temperature storage test indicating the same gassing mechanism.

Conclusions

The main theories surrounding the mechanism behind LTO gas formation were tested in LTO/LMO multi-layer pouch cells through high temperature storage testing and high temperature cycling. The theory that $LiPF_6$ decomposing into HF being the main source of gas was disputed by replacing the salt in two different salt replacement formulations. The data showed that TFSI and FSI as salt replacements caused an increase in gas formation compared to $LiPF_6$. While LiFSI did manage to change the

composition of gas formed more drastically than other formulations, it produced significantly more CO_2 and had poor performance in all tests conducted. The salt replacement of LiTFSI showed high temperature storage benefits, but worse cycling performance in addition to producing more gas of the same composition as the baseline with $LiPF_6$. Both provide evidence that the $LiPF_6$ breakdown due to reaction with moisture is not the main source of gassing and removing the salt is not a practical or effective solution. The theory that the gas formation is due to HF as an impurity in the electrolyte or as an impurity on the LTO was tested through use of DMAc as an acid scavenger. It was proven through electrolyte storage testing that this additive does scavenge acid until the additive has been consumed. Despite its HF scavenging abilities, this formulation had the most gas formed with no change in the amount of hydrogen produced after storage compared to the baseline indicating that HF and water impurities in the electrolyte is not the main source of gassing, and water influence is the same in this system and is any other system; not as a main source of gas. The final theory of the electrolyte interacting with the surface of the LTO was tested through an SEI forming additive, TMSB, and through an EC free formulation. Both formulations reduced the amount of gas formed after formation, high temperature storage, and high temperature cycling. Though TMSB showed large gas reduction compared to the baseline and other formulations despite minimal performance losses. This data showed strong evidence that an SEI is an efficient and cost-effective way of decreasing the gas formed in the LTO system, and that TMSB is a good additive to do so. EC free electrolyte displayed superior cycling performance and decreased gassing after formation and high temperature cycling compared to that

of the baseline indicating that EC free is complimentary to the LTO anode and not necessary for 45°C performance. The EC removed from this system was replaced with PC, which showed it showed should be kept in smaller amounts than what is used here as it started to decompose at 60°C. The change in gas volume, gas composition, and performance highlighted the role solvent choice has in the LTO system and supports the theory that the main source of gassing in LTO is reactions between the solvent and the electrode surface. Ongoing work is looking into the more of the individual solvent interactions with the LTO surface and investigations into the source of the hydrogen through deuterated isotopic labelling gas analysis. In addition to this, new additives are being investigated and XPS is being used to determine the optimal SEI.

References

1. Ferg, E.; Gummow, R.J.; de Kock, A.; Thackeray, A.M.M., Spinel Anodes for Lithium Ion Batteries, *Journal of the Electrochemical Society* **1994,** *141*, L147-L150.
2. Ohzuku, T.; Ueda, A.; Yamamoto, N., Zero-Strain Insertion Material of $Li[Li_{1/3}T_{5/3}]O_4$ for Rechargeable Lithium Cells, *Journal of the Electrochemical Society* ***1995,*** *142,* 1431-1435.
3. Aldon, L.; Kubiak, P.; Womes, M.; Jumas, J.C.; Olivier-Fourcade, J.; Tirado, J.L.; Corredor, J.I.; Pérez Vicente, C., Chemical and Electrochemical Li-Insertion into the $Li_4Ti_5O_{12}$ Spinel, *Chemical* Materials **2004,** *16*, 5721–5725.
4. Sandhya, C.P.; John, B.; Gouri, C., Lithium Titanate as Anode Material for Lithium-Ion Cells: A Review, *Ionics* **2017,** *20*, 601-620.
5. Colbow, K.W.; Dahn, J.R.; Haering, R.R., Structure and Electrochemistry of the Spinel Oxides $LiTi_2O_4$ and $Li_{4/3}Ti_{5/3}O_4$, *Journal of Power Sources* **1989,** *26*, 397-402.
6. Wu, K.; Yang, J.; Zhang, Y.; Wang, C.; Wang, D., Investigation on $Li_4Ti_5O_{12}$ Batteries Developed for Hybrid Electric Vehicle, *Journal of Applied Electrochemistry* **2012**, *42*, 989-995.
7. Kai, W.; Yang, J.; Liu, Y.; Zhang, Y.; Wang, C.; Xu, J.; Ning, F.; Wang, D., Investigation on Gas Generation of $Li_4Ti_5O_{12}/LiNi_{1/3}Co_{1/3}Mn_{1/3}O_2$ Cells at Elevated Temperature, *Journal of Power Sources* **2013**, *237*, 285-290.
8. Liu, J.; Bian, P.; Li, J.; Ji, W.; Hao, H.; Yu, A., Gassing Behavior of Lithium

Titanate Based Lithium Ion Batteries with Different Types of Electrolytes, *Journal of Power Sources* **2015,** *286,* 380-387.

9. Wang, Q.; Zhang, J.; Liu, W.; Xie, X.; Xia, B., Quantitative Investigation of the Gassing Behavior in Cylindrical $Li_4Ti_5O_{12}$ Batteries, *Journal of Power Sources* **2017**, *343,* 564-570.
10. Burns, J.C.; Sinha, N.N.; Jain, G.; Ye, H.; Van Elzen, C.M.; Scott, E.; Xiao, Z.; Lamanna, W.M.; Dahn, J.R.,The Impact of Intentionally Added Water to the Electrolyte of Li-Ion Cells with Lithium Titanate Negative Electrodes, *Journal of the Electrochemical Society* Soc. **2014**, *3,* A247-A255.
11. Zhou, H.; Fang, Z.; Li, J., $LiPF_6$ and Lithium Difluoro(oxalato)borate/Ethylene Carbonate + Dimethyl Carbonate + Ethyl(methyl)carbonate Electrolyte for $Li_4Ti_5O_{12}$ Anode, *Journal of Power Sources* **2013,** *230,* 148-154.
12. Tebbe, J.; Fuerst, T.F.; Musgrave, C.B.; Mechanism of Hydrofluoric Acid Formation in Ethylene Carbonate Electrolytes with Fluorine Salt Additives, *Journal of Power Sources* **2015,** *297,* 427-435.
13. Lux, S.F.; Lucas, I.T.; Pollak, E.; Passerini, S.; Winter, M.; Kostecki, R., The Mechanism of HF Formation in $LiPF_6$ Based Organic Carbonate Electrolytes, *Electrochemistry Communications* **2012,** *14,* 47-50.
14. Campion, C.; Li, W.; Lucht, B., Thermal Decomposition of $LiPF_6$-Based Electrolytes for Lithium-Ion Batteries, *Journal of the Electrochemical Society* **2005**, *152,* A2327-A2334.
15. He, Y.; Li, B.; Liu, M.; Zhang, C.; Lv, W.; Yang, C.; Li, J.; Du, H.; Zhang, B.; Yang, Q.; Kim, J.; Kang, F., Gassing in $Li_4Ti_5O_{12}$-Based Batteries and Its

Remedy, *Scientific Reports* **2012,** *913*, 1-9.

16. Gao, J.; Gong, B.; Zhang, Q.; Wang, G.; Dai, Y.; Fan, W., Study of the Surface Reaction Mechanism of $Li_4Ti_5O_{12}$ Anode for Lithium-Ion Cells, *Ionics* **2015**, *21*, 2409-2416.
17. Aiken,C.P.; Xia, J.; Wang, D.Y.; Stevens, D.A.; Trussler, S.; Dahn, J.R., An apparatus for the study of in situ gas evolution in Li-ion Pouch Cells, *Journal of the Electrochemical Society* **2014,** *161*, A1548-A1554.

Figures

Figure 2.1

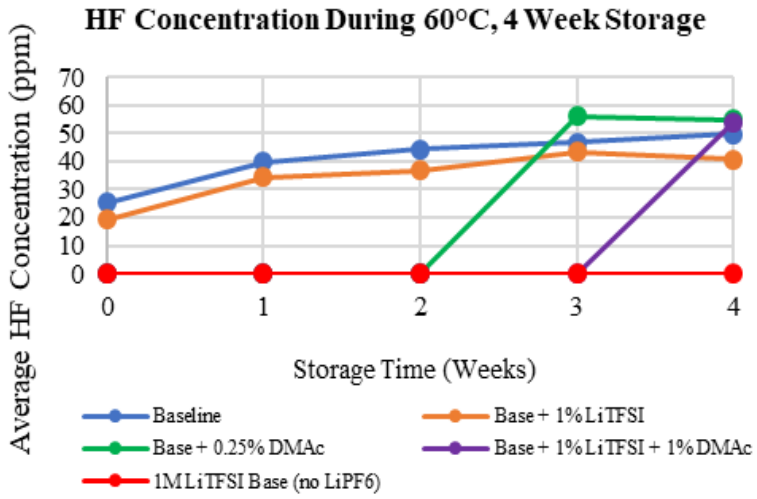

Fig. 2.1: Electrolyte sealed under nitrogen in aluminum bottles was stored in 60°C for four weeks. At each week interval, one electrolyte bottle from each formulation was pulled out and underwent HF testing through Karl Fischer titration.

Figure 2.2

a)

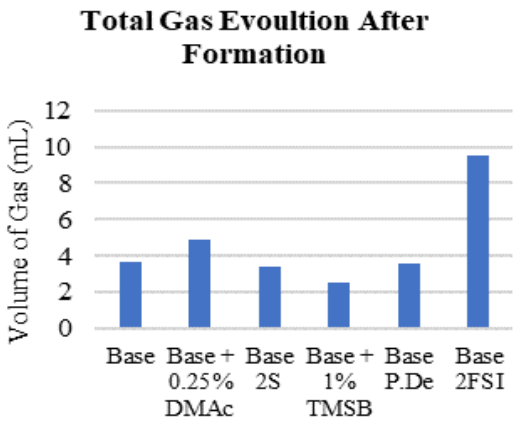

b)

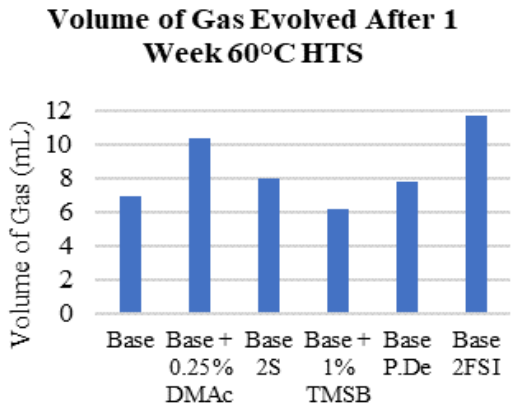

Figure 2.2: Volume of gas evolved from pouch cells after a) 45°C, 12-hour formation including aging and b) high temperature storage for 1 week**.**

Figure 2.3

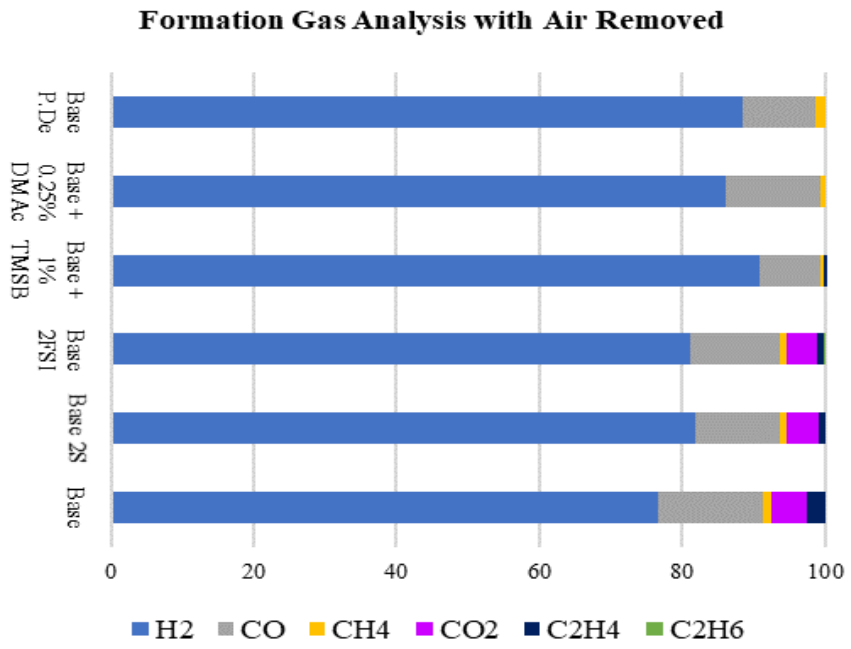

Figure 2.3: Pouch cells underwent formation and 45°C, 12-hour aging before the gas was extracted under inert atmosphere with a gas tight syringe. Gas samples were injected into the GC-TCD for gas analysis.

Table 2.1

Volume of Gases Formed After Formation and Aging								
Electrolyte	H2 (mL)	CO (mL)	CH4 (mL)	CO2 (mL)	C2H4 (mL)	C2H6 (mL)	C3H6 (mL)	C3H8 (mL)
Base	2.797	0.540	0.040	0.178	0.095	-	-	-
DMAC	4.234	0.657	0.028	-	-	-	-	-
2S	2.804	0.402	0.034	0.152	0.033	-	-	-
TMSB	2.261	0.214	0.011	-	0.014	-	-	-
P.De	3.168	0.363	0.049	-	-	-	-	-
2FSI	7.723	1.202	0.086	0.395	0.106	0.016	-	-

Table 2.1: Using the data from the gas composition and gas volume measurements, the exact amount of each gas produced after formation and aging was calculated for comparison.

Table 2.2

Volume of Gases Formed After 1 Week at 60°C								
Electrolyte	H2 (mL)	CO (mL)	CH4 (mL)	CO2 (mL)	C2H4 (mL)	C2H6 (mL)	C3H6 (mL)	C3H8 (mL)
Base	4.690	0.939	0.065	0.686	0.450	0.057	-	-
DMAC	7.360	1.693	0.127	0.843	0.295	-	-	-
2S	5.673	1.444	0.070	0.642	0.098	0.048	-	-
TMSB	4.458	1.160	0.038	0.314	0.117	0.080	-	-
P.De	5.831	1.042	0.089	0.211	0.104	0.056	0.409	0.005
2FSI	5.569	2.215	0.183	3.482	0.026	0.211	-	-

Table 2.2: Using the data from the gas composition and gas volume measurements, the exact amount of each gas produced after one week of high temperature storage was calculated and compared.

Figure 2.4

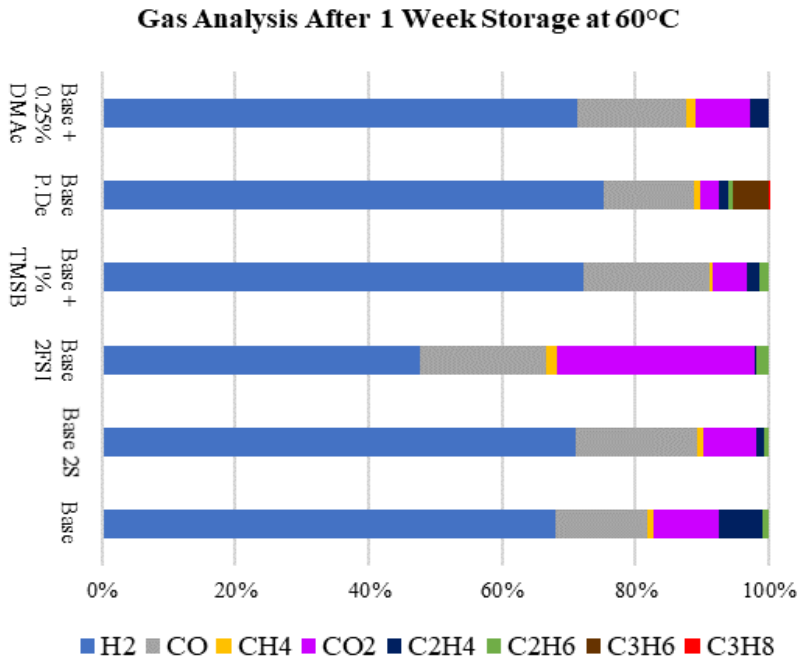

Figure 2.4: Pouch cells were degassed after formation and stored at 60°C for 1 week at 100% SOC. After storage, gas was extracted under inert atmosphere with a gas tight syringe and injected into the GC-TCD for analysis.

Figure 2.5

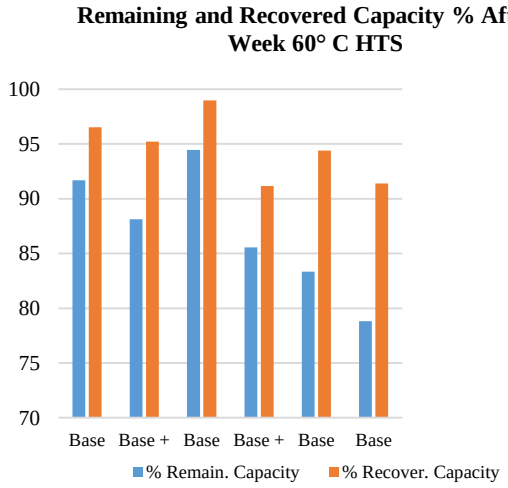

Figure 2.5: Remaining and recovered capacity percentage for pouch cells after 1 week at 60°C at 100% SOC.

Figure 2.6

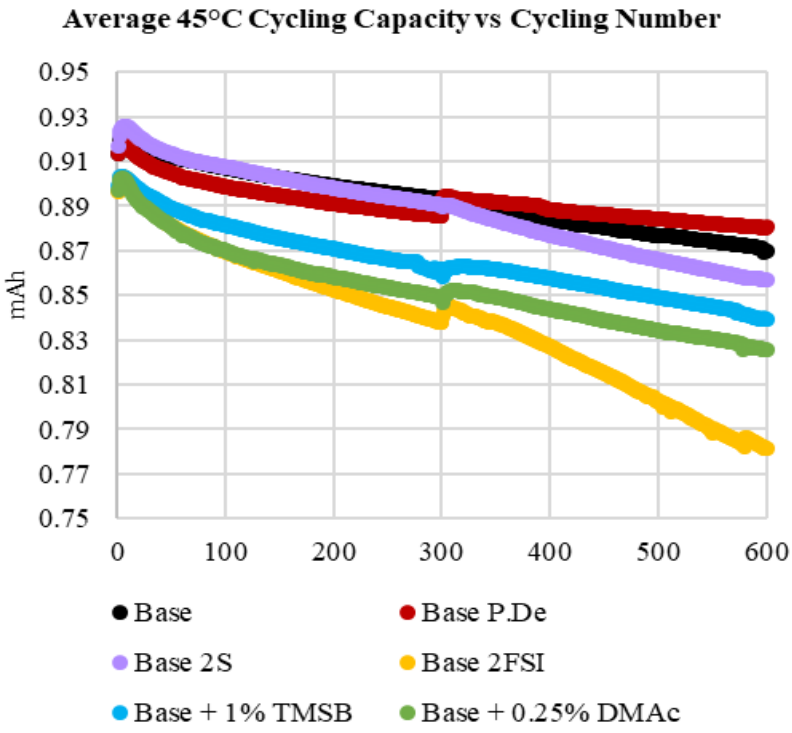

Figure 2.6: Capacity retention after 500 cycles at 45°C. At 300 cycles cells are paused and taken out for gas volume measurement before being restarted.

Figure 2.7

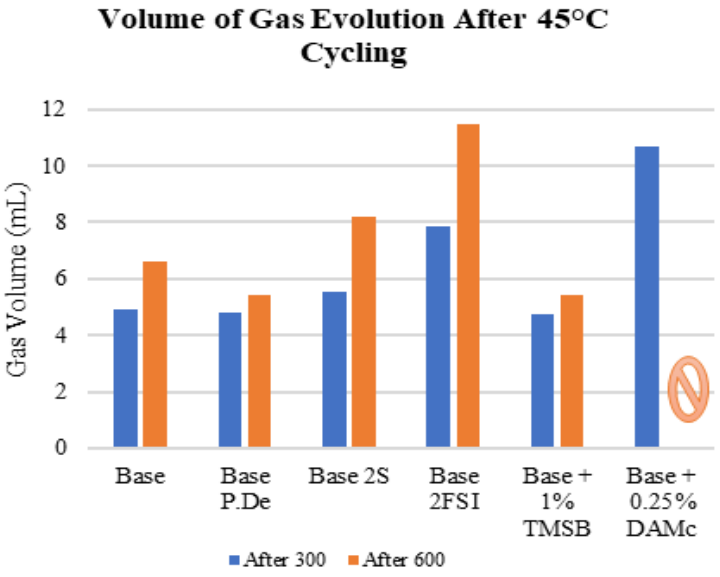

Figure 2.7: After 300 and 600 cycles the gas volume of each pouch cell was measured at room temperature. The 0.25% DMAc formulation was not able to be measured due to floating cells from too much gas formed.

CHAPTER 3

THE EFFECTS OF ELECTROLYTE ADDITIVES ON Li4Ti5O12 AND HOW THEY IMPACT GASSING

By

Mickdy Milien[2]; Jennifer Hoffmann[1,3]; Martin Payne[3]; Brett Lucht[4]

Manuscript Pending Publication in Journal of Electrochemistry

[1]PhD candidate, Department of Chemistry, The University of Rhode Island, Kingston, RI 02882.

[2]PhD graduate, Department of Chemistry, The University of Rhode Island, Kingston, RI 02882.

[3]Battery R&D, Gotion Inc., Independence, Ohio 44131, USA

[4]Professor, Department of Chemistry, The University of Rhode Island, Kingston, RI, 02882.

Abstract

For lithium ion batteries, $Li_4Ti_5O_{12}$ (LTO) as an anode material presents many advantages over the carbon anode most widely used in commercial applications today. With improved safety, long cycle life, and zero volumetric variation it is reasonable that this material would be sought after for the high power, electric vehicle applications.[1,3] However, at elevated temperature ranges LTO suffers extreme gas formation due to interfacial side reactions at the surface.[5-7,12] To mitigate these reactions, several classes of electrolyte additives have been investigated in full cell $Li_4Ti_5O_{12}/LiMn_2O_4$ coin cells and pouch cells in this work. ATR-IR and X-ray photoelectron spectroscopy has been used to gain an understanding of the surface films formed with different additives while in-situ gas measurements based on Archimedes' principle and gas chromatography have given insight into how the implementation of these additives affects gassing. Through this information, an additive that successfully reduced the gassing and a detailed look into the characterization of an ideal SEI for LTO anode is presented.

Introduction

Graphite is the most ubiquitous anode material used in lithium ion batteries (LIB) when it comes to high energy density applications because of its low operating potential, low cost, and reasonable lifetime in standard conditions (moderate rates and temperature).[1] When it comes to high power density LIB such as those required for power tools, start-stop engines, or regenerative breaking, graphite is not suitable because of its limited rate capability and the safety concerns (lithium plating) associated with fast charging.[2-3] Intrinsic characteristics of $Li_4Ti_5O_{12}$ (LTO) such as its high reduction potential (1.55 V vs. Li/Li^+) and lack of volume change during insertion/extraction (< 1%) coupled with the fact that its synthetic route has been optimized to render robust high rate capabilities and cycling stability makes LTO a very favorable anode material for high powered LIB.[1, 3-4] Because LTO's high working potential narrows the voltage window of cells when paired with conventional cathode materials, LTO is currently most suitable for high-powered applications. The principal challenge associated with the use of LTO anodes is the gassing of cells containing LTO both at elevated temperatures and when stored in the charged state.[3, 5-7]

Qin et. al reported that the predominant gas detected was H_2, the amount increased with temperature, and was only generated in cells containing LTO in the charged state.[8] Storage experiments of LTO in the charged state with and without $LiPF_6$ salt, also performed by Qin et. al., revealed that the amount of H_2 generated was reduced significantly in the absence of $LiPF_6$. Gassing measurements reported by Belharouck et. al. depicted an inverse relationship between H_2 generation and alkyl gasses generated from electrolyte decomposition.[9] Since gaseous electrolyte

decomposition products are likely to be accompanied by insoluble electrolyte decomposition products, which passivate the surface of LTO, this suggests that passivation of the electrode would decrease gassing. In addition to confirming more gassing at a higher state of charge, Liu et. al also demonstrated that cells stored in the presence of PC had less gassing than cells stored in the presence of EC.[5] This was attributed to the fact that the PC-based electrolyte formed thicker and denser SEI layers on LTO surfaces than EC-based electrolytes. While the presence of trace amounts of water in the electrolyte or the electrode was initially deemed the contributing factor to H_2 generation, the results all reveal that the contact of the electrolyte with the charged surface of LTO is the problem. Various techniques such as coating, doping, poisoning, or passivating the surface of LTO to reduce gassing have been attempted.[8-10,12] This work focuses on using 2 classes of electrolyte additives (imides and borates) to passivate the surface of LTO and to employ both *in situ* and *ex situ* gassing measurements as well as *ex situ* surface analysis to gain an understanding of the effects of the additives.

Experimental

Materials

Battery grade ethylene carbonate (EC), propylene carbonate (PC), diethyl carbonate (DEC), lithium hexafluorophosphate ($LiPF_6$), LiTFSI, LiFSI, LiBOB, and LiDFOB were provided by BASF and used as received. TMSB was purchased from Sigma Aldrich and used as received.

Cell Preparation

Pouch cells **–** 920 mAh multilayer pouch cells were assembled by SKC using commercially available BTBM LMO as the cathode material and commercially available POSCO LTO as the anode material. The cells were dried at 55 °C for 12 hours under vacuum prior to filling. Once dried, cells were transferred to an argon glove box and filled with 9.1 g of electrolyte, Base = 1.0 M LiPF6 in EC/PC/DEC (15:20:65), and vacuum sealed. All cells undergo 12 hours of rest at 25 °C after sealing to ensure complete wetting. Cycling data and gas measurements were obtained from pouch cells.

Coin cells – Full cell coin cells were assembled using the same commercially available BTBM LMO cathode material and the commercially available POSCO LTO anode material that was used in the pouch cells. Electrodes were dried at 85°C for 12 hours under vacuum prior to assembly. Once dried, cells were transferred to a nitrogen glove box and assembled using PRED 2032 type coin cell parts, Celgard polypropylene separator, and 120 µl of electrolyte. Cells underwent 1 hour of resting at 25°C after assembly to ensure complete wetting before formation and cell testing. Surface analysis was carried out on electrodes extracted from coin cells.

Electrochemical Testing

Formation and Aging **–** Pouch cells were clamped and cycled with a constant current (CC) charge at 0.1C with a 2.8 V cutoff voltage using a MACCOR battery cycler. Once charged, the cells were unclamped and placed in a 45 °C chamber for 12 hours of aging. Cells were then degassed and vacuum-sealed in the argon glove box before

undergoing a second formation step in which the cells were cycled with a constant current-constant voltage (CC-CV) charge and CC discharge between 2.8 and 1.7 V vs. $Li_4Ti_5O_{12}/Li_7Ti_5O_{11}$ with the following procedure: 1 cycle at C/10, 1 cycle at C/5, and 1 cycle at 1C. Coin cells did not undergo a degassing step like the pouch cells but otherwise followed the same formation and aging steps.

High Temperature Storage (HTS) **–** After completing the formation and aging procedure cells were clamped tightly and underwent the following before storage procedure: charged with CC-CV to 2.8 V at 0.7C with a cutoff current of 0.02C, discharged with CC to 1.7 V at 1C, and charged with CC-CV to 2.8 V at 0.7 C with a cutoff current of 0.02C. The cells were then stored in the 100% state of charge (SOC) in a 60 °C chamber for 1 week. Upon completing the storage procedure cells followed the following after storage procedure: discharged with CC to 1.7 V at 1C, charged with CC-CV to 2.8 V and finally discharged to 1,7 V at 1C.

Long Term Cycling **–** After completing the formation and ageing procedure, cells undergo rate testing between 2.8 and 1.7 V according to the following procedure: 2 cycles with C/2, D/2; 1 cycle with C/2, D/5; 1 cycle with C/2, D/2; 1 cycle with C/2, 1D; 1 cycle with C/2, 2D; and 3 cycles with C/2, D/2 (where C = charge rate and D = discharge rate). Once the rate testing is complete, cells undergo the before storage procedure described in the HTS section, stored in the 100% SOC for 24 hours, and undergo the after-storage procedure described in the HTS section. Cells were transferred to a 45 °C chamber (tightly clamped) and cycled between 2.8 and 1.7 V at 1C with a C/10 cycle every 50 cycles.

All cells were prepared in duplicate to confirm reproducibility. Representative data are presented.

Gas Analysis

Gas Volume – Gas volume was measured before first formation, before aging after first formation, after aging before degassing, before storage and/or cycling, and after storage and/or cycling according to the procedure first described by Aiken et al. The pouch cells were hung from the bottom of scale and tarred. After reaching a stable zero, the cells were submerged completely to a defined level in 25°C deionized water. The recorded weight of the cell while submersed was then used along with the Archimedes' principle to calculate the amount of gas evolved over time[11].

Gas Composition – To measure the composition of gasses, cells were brought into the argon dry box for extraction. A 0.5 mL Vici precision sampling analytical pressure-lok syringe was used to manually extract the gas sample from the cell under argon atmosphere. The sample was then manually injected into a Varian 450 gas chromatograph equipped with a 19808 ShinCarbon ST column, thermal conductivity detector (TCD), and an argon carrier gas.

Surface Analysis

X ray Photoelectron Spectroscopy –The cells were disassembled in an argon glove box. The electrodes were rinsed with dimethyl carbonate (DMC) three times to remove residual EC and $LiPF_6$ and evacuated overnight prior to surface analysis. X-ray photoelectron spectroscopy (XPS) was acquired with a Thermo K-alpha system

using Al Kα radiation (hυ = 1486.6 eV) under ultra-high vacuum and a measured spot size of 400 μm, and a 50.0 eV pass energy for the detector. Samples were transferred into the XPS chamber with a vacuum transfer vessel. The binding energy was corrected based on the C 1s of C-C at 284.3 eV. The spectra obtained were analyzed using Thermo Advantage software (version 5.926). A mixture of 30% Laurentzian and 70% Gaussian functions was used for the least-squares curves fitting procedure.

Results and Discussion

Although gasses formed during formation are typically removed from cells, gas analysis was carried out after formation and aging with the various electrolyte formulations to compare the effects the various additives had on gassing. The results are depicted in Figure 3.2. The average gas volume for each formulation is displayed on the left and the gas composition for the corresponding electrolyte formulation is displayed on the right. With the exception of 2.0 wt. % LiBOB the predominant gas observed is H_2. Pouch cells with 1.0 wt. % TFSI, 1.0 wt. % LiBOB, 2.0 wt. % LiBOB, and 1.0 wt. % TMSB all generated less gas than the Base electrolyte, while cells cycled with 1.0 wt. % FSI and 1.0 wt. % DFOB generated more gas than the Base electrolyte. With an 88.72 % reduction in gas, cells with 2.0 wt. % LiBOB had the biggest impact on the volume of gas generated after formation and aging. With the exception of 2.0 wt. % LiBOB, the predominate gas detected after formation and aging was H_2 (consistent with what has been reported in literature).[1,6] The amount of CO_2 detected increased in the presence of the oxalato borates, which are known to generate CO_2.[12]

XPS surface analysis was employed to characterize the surface of LTO electrodes after formation and aging with the various electrolyte formulations. Figure 3.3 displays the relative atomic concentrations of LTO anodes after formation and aging with all the electrolyte formulations. Thin surface films (indicated by the Ti2p concentration) were detected on the surface of LTO in the presence of the Base electrolyte, 1.0 wt. % TFSI, and 1.0 wt. % FSI. Although thicker boron containing surface films were detected on the surface of LTO in the presence of the borates, 1.0 wt. % TMSB generated the thinnest film of the borates. In addition to thicker surface films LTO, which underwent formation and aging with the oxalato borates (1.0 wt. % LiBOB, 2.0 wt. % LiBOB, and 1.0 wt. % DFOB) all display less phosphorous and fluorine concentrations. This indicates less $LiPF_6$ decomposition in the presence of the borates.

Figure 3.4 provides C1s, O1s, and F1s core spectra of LTO electrodes extracted from cells after formation and aging with the Base electrolyte and the Base + borate additives (1.0 wt. % LiBOB, 2.0 wt. % LiBOB, 1.0 wt. % DFOB, and 1.0 wt. % TMSB). The surface of LTO anodes cycled with the Base electrolyte displays the thinnest film (based on the metal oxide peak (530.2 eV) in the O1s spectrum), which consists of electrolyte decomposition products Li_2CO_3 and LiF (290 eV, C1s and 685 eV F1s, respectively). The thinnest surface film of the borates was detected with 1.0 wt. % TMSB, which consists of LiF and TMSB-derived species (based on the B1s concentration, see figure 3). The thickest surface films consisting of oxalates and LiF were observed in the presence of the oxalato borates. Due to the fact that DFOB

contributes to the generation of LiF, LTO electrodes cycled with 1.0 wt. % DFOB contained more LiF than those cycled with either concentration of LiBOB.

Since gassing of cells containing LTO are reported to be a result of the instability of the electrolyte on the charged surface of LTO at elevated temperatures, cells which have undergone the formation and aging procedure with the various additive-containing electrolyte formulations, degassed, and resealed were stored in the 100% SOC for 1 week at 60 °C. The results are depicted in Figure 3.5. The average gas volume is displayed on the left, while the gas composition is displayed on the right. As far as the volume of gas generated, pouch cells with 1.0 wt. % TMSB were the only ones that reduced gassing after storage. Incorporating 1.0 wt. % of TMSB into the Base electrolyte decreased gassing by 5.22% after 1 week of storage at 60 °C. As far as gas composition, the predominant gas detected irrespective of the electrolyte formulation used was H_2. Cells that were stored for 1 week with the oxalato borates generated more CO_2 than the others, while the alkyl gasses (CH_4, C_2H_4, and C_2H_6) were only detected in the absence of the oxalato borates. This suggests that while incorporating the oxalato borates into the Base electrolyte contributes to CO_2 generation, it also hinders parasitic reactions with the electrolyte solvents.

In order to gain insight into the composition of the surface film on LTO anodes after 1 week of storage at 60 °C XPS surface analysis was performed on LTO electrodes extracted from cells that have been stored with the various electrolyte formulations. Based on the concentration of titanium, the thinnest surface film was detected on the LTO anode stored with 1.0 wt. % FSI, the thickest surface films were detected on LTO anodes stored with the oxalato borates, and LTO anodes stored with

1.0 wt. % TMSB had the thinnest surface film of all cells stored with the borates. Manganese was only detected on the surface of LTO anodes stored in the absence of the borate additives. This suggests that the borate additives prevented manganese dissolution from the LMO cathodes during 1 wee of storage at 60 °C.

C1s, O1s, and F1s core spectra of LTO anodes extracted from cells after 1 week of storage at 60 °C are displayed in Figure 3.7. A thin surface film (based on the intensity of the metal oxide peak; 530.2 eV, O1s) consisting of LiF (685 eV, F1s) was detected on the LTO anode stored with the Base electrolyte. LTO anodes stored with 1.0 wt. % FSI had the thinnest surface film, which consisted of LiF. The thickest surface film consisting of oxalates and LiF was detected on the surface of LTO anodes stored with 1.0 wt. % LiBOB. LTO anodes stored with 1.0 wt. % DFOB displayed a thick surface film consisting of oxalates and LiF. Cells stored with 1.0 wt. % TMSB had the thinnest surface film of the borates, which consisted of TMSB-derived species (B1s).

While the focus of this work was to determine if and how the use of electrolyte additives to passivate LTO anodes affects gassing, the impact of the additives on cycling stability should not be overlooked. For this reason, LTO/LMO pouch cells were assembled with the various electrolyte formulations and cycled at 45 °C for 600 cycles. The cells underwent 1 cycle at a 0.1C rate (formation), degassed, and re-sealed. The remaining cycles were carried out at a 1C rate, and the resulting cycling performance is shown in Figure 3.8a. Although cells cycled with 1.0 wt. % FSI displayed the best performance of all the additives, it was on par with the performance observed with the Base electrolyte. Cells cycled with 1.0 wt. % TFSI, 1.0 wt. %

LiBOB, and 1.0 wt. % DFOB had less capacity than cells cycled with the Base electrolyte prior to 300 cycles, however cells cycled with 1.0 wt. % LiBOB and 1.0 wt. % TFSI had similar capacities to cells cycled with the Base electrolyte after 600 cycles. Increasing the concentration of LiBOB by 1.0 wt. % resulted in a drop in capacity and cells cycled with 1.0 wt. % TMSB displayed the worst capacity of all the additives. Capacity retention is plotted in Figure 3.8b. Conversely to the cycling performance, cells cycled with the oxalato borates outperformed those cycled with the imides as far as capacity retention is concerned. Cells cycled with the formulations which formed the thinnest surface films (1.0 wt. % FSI, 1.0 wt. % TFSI, and 1.0 wt. % TMSB) displayed the most capacity fading, while those cycled with the oxalato borates displayed the least fading. This clearly demonstrates that passivating the surface of LTO is beneficial to cycling stability. It should be noted that the spikes observed during cycling are a result of the cells being stopped for gassing measurements and resumed afterwards.

The volume of gas evolved during cycling was measured after 300 cycles and again after 600 cycles. The results are displayed in Figure 3.9. While cells cycled with 1.0 wt. % LiBOB and 1.0 wt. % TMSB both generated less gas than cells cycled with the Base electrolyte after 300 cycles, cells cycled with 1.0 wt. % TMSB were the only ones that displayed reduced gassing after 600 cycles.

Conclusion

While better cycling capacity was observed in the presence of the imides, the thinnest surface films were observed resulting in faster capacity fading and more gassing. The oxalato borates formed the thickest surface films, and less H_2 was

detected, however the oxalato borates are known for generating CO_2, thus gassing is not reduced overall. Less gassing was detected in the presence of TMSB in all cases, however TMSB displays the worst capacity retention of all the additives. The presence of the alkyl gasses, LiF, and $Li_xPO_yF_z$ combined with the pronounced fading observed with TFSI, FSI, and TMSB suggests that these additives react with the electrolyte. Nonetheless, the goal of reducing LTO gas was achieved in the presence of TMSB. Optimization of additive concentration and further experiments are underway.

References

1. Han, C.; He, Y.-B.; Liu, M.; Li, B.; Yang, Q.-H.; Wong, C.-P.; Kang, F., A review of gassing behavior in Li4Ti5O12-based lithium ion batteries. *J. Mater. Chem. A* **2017,** *5* (14), 6368-6381.

2. Goodenough, J. B., Rechargeable batteries: challenges old and new. *Journal of Solid State Electrochemistry* **2012,** *16* (6), 2019-2029.

3. Xu, G.; Han, P.; Dong, S.; Liu, H.; Cui, G.; Chen, L., Li 4 Ti 5 O 12 -based energy conversion and storage systems: Status and prospects. *Coordination Chemistry Reviews* **2017,** *343*, 139-184.

4. Chen, S.; Xin, Y.; Zhou, Y.; Ma, Y.; Zhou, H.; Qi, L., Self-supported Li4Ti5O12 nanosheet arrays for lithium ion batteries with excellent rate capability and ultralong cycle life. *Energy & Environmental Science* **2014,** *7* (6).

5. Liu, J.; Bian, P.; Li, J.; Ji, W.; Hao, H.; Yu, A., Gassing behavior of lithium titanate based lithium ion batteries with different types of electrolytes. *Journal of Power Sources* **2015,** *286*, 380-387.

6. Lv, W.; Gu, J.; Niu, Y.; Wen, K.; He, W., Review—Gassing Mechanism and Suppressing Solutions in Li4Ti5O12-Based Lithium-Ion Batteries. *Journal of The Electrochemical Society* **2017,** *164* (9), A2213-A2224.

7. He, M.; Castel, E.; Laumann, A.; Nuspl, G.; Novák, P.; Berg, E.J., In Situ Gas Analysis of $Li_4Ti_5O_{12}$ Based Electrodes at Elevated Temperatures. *Journal of The Electrochemical Society* **2015,** *162* (6), A870-A876.

8. Qin, Y.; Chen, Z.; Belharouak, I.; Amine, K., Mechanism of LTO gassing and potential solutions. **2011**

9. Belharouak, I.; Koenig, G.M.; Tan, T.; Yumoto, H.; Ota, N.; Amine, K., Performance degradation and gassing of $Li_4Ti_5O_{12}/LiMn_2O_4$ Lithium-Ion Cells. *Journal of the Electrochemical Society* **2012,** *159* (8), A1165-A1170.

10. Li, X.; Zhao, X.; Huang, P.-x; Wang, M.-s; Huang, Y.; Zhou, Y.; Lin, T.-h; Qu, M.-z; Yu, Z.-1., Enhanced electrochemical performance of SrF2-modified Li4Ti5O12 composite anode materials for lithium-ion batteries. *Journal of Alloys and Compounds* **2017,** 693, 61-69.

11. Aiken, C.P.; Xia, J.; Wang, D.Y.; Stevens, D.A.; Trussler, S.; Dahn, J.R., An apparatus for the study of in situ gas evolution in Li-ion pouch cells, *Journal of Electrochemical Society* **2014,** 161, A1548-A1554.

12. Lu, Q.; Fang, J.; Yang, J.; Feng, X.; Wang, J.; Nuli, Y., A polyimide ion-conductive protection layer to suppress side reactions on $Li_4Ti_5O_{12}$ electrodes at elevated temperature. *RSC Adv.* **2014,** *4*, 10280-10283.

13. Xu, M.; Tsiouvaras, N.; Garsuch, A.; Gasteiger, H.A.; Lucht, B.L., Generation of Cathode Passivation Films via Oxidation of Lithium Bis(oxalato) Borate on High Voltage Spinel ($LiNi_{0.5}Mn_{1.5}O_4$). *The Journal of Physical Chemistry* **2014,** *118* (14), 7363-7368.

14. Bodenes, L.; Dedryvere, R.; Martinez, H.; Fischer, F.; Tessier, C.; Peres, J. P., Lithium-Ion Batteries Working at 85 C: Aging Phenomena and Electrode/Electrolyte Interfaces Studied by XPS. *Journal of the Electrochemical Society* **2012,** *159* (10), A1739-A1746

15. Banerjee, A.; Shilina, Y.; Ziv, B.; Ziegelbauer, J. M.; Luski, S.; Aurbach, D.; Halalay, I. C., Review—Multifunctional Materials for Enhanced Li-Ion Batteries

Durability: A Brief Review of Practical Options. *Journal of The Electrochemical Society* **2017,** *164* (1), A6315-A6323.

16. Delp, S.A.; Borodin, O.; Olguin, M.; Eisner, C.G.; Allen, J.L.; Jow, T.R., Importance of reduction and oxidation stability of high voltage electrolytes and addtives. *Electrochimica Acta* **2016,** *209*, 498-510.

17. Wang, K.; Xing, L.; Yunmin, Z.; Zheng, X.; Cai, D.; Li, W.; A comparative study of Si-containing electrolyte additives for lithium ion battery: which one is better and why is it better. *Journal of Power Sources* **2017,** *342*, 677-684

18. Yan, C.; Xu, Y.; Xia, J.; Gong, C.; Chen, K., Tris(trimethylsilyl)borate as an electrolyte additive for high-voltage lithium ion batteries using $LiNi_{1/3}Co_{1/3}O_2$ cathode. *Journal of Energy Chemistry* **2016,** *25*, 659-666.

Figure 3.1

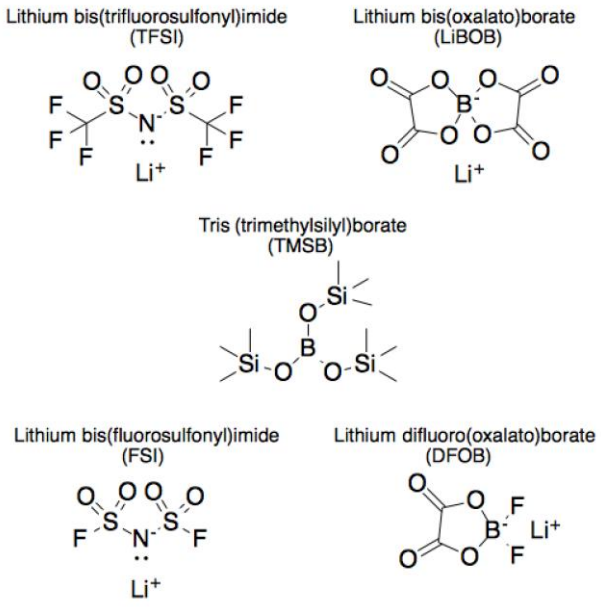

Figure 3.1: Chemical Structures of LiTFSI (TFSI), LiFSI (FSI), LiBOB, TMSB, and LiDFOB (DFOB).

Figure 3.2

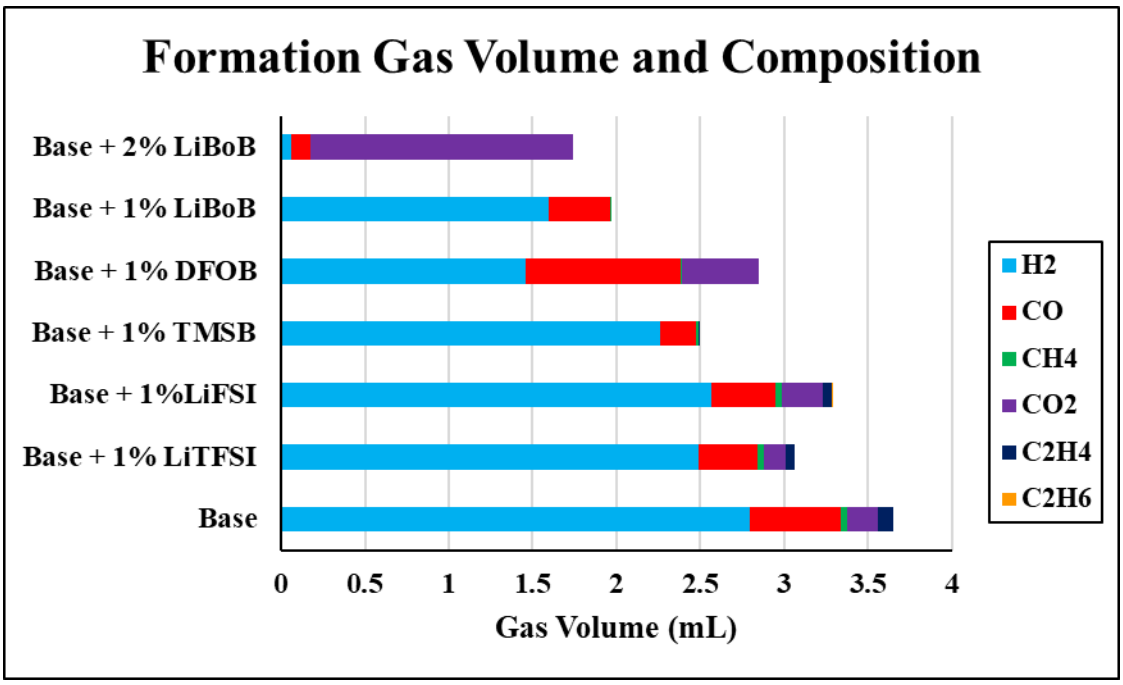

Figure 3.2 - Average volume of gas (left) and composition of gas generated after formation and ageing with the Base electrolyte, Base + 1.0 wt % TFSI, Base + 1.0 wt % FSI, Base + 1.0 wt % LiBOB, Base + 2.0 wt % LiBOB, Base + 1.0 wt % DFOB, and Base + 1.0 wt % TMSB.

Figure 3.3

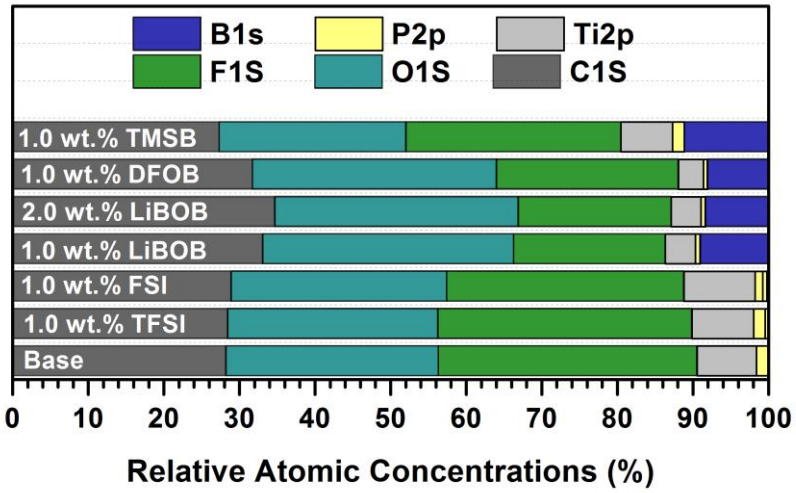

Figure 3.3 - Relative atomic concentrations of elements detected on the surface of LTO electrodes after formation and aging with the Base electrolyte, Base + 1.0 wt % TFSI, Base + 1.0 wt % FSI, Base + 1.0 wt % LiBOB, Base + 2.0 wt % LiBOB, Base + 1.0 wt % DFOB, and Base + 1.0 wt % TMSB.

Figure 3.4

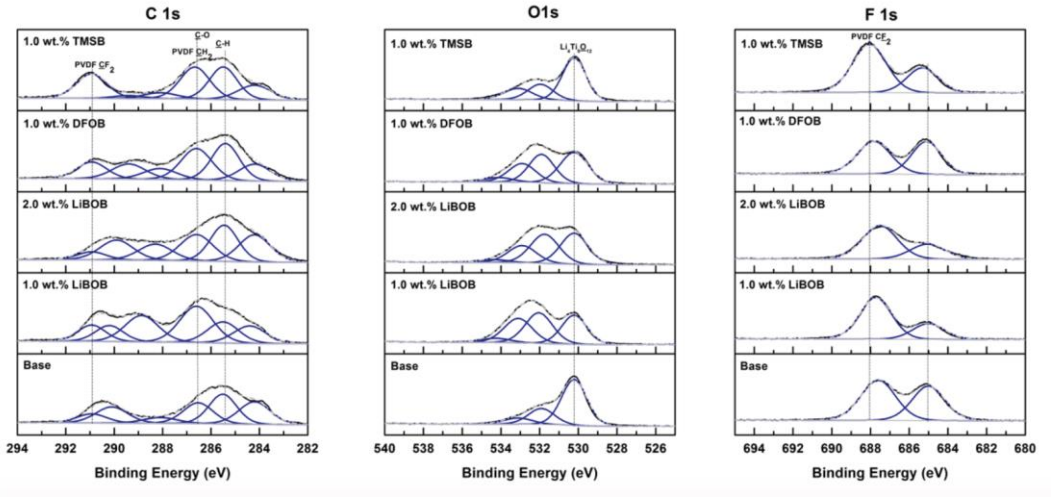

Figure 3.4: C 1s, O 1s, and F 1s core spectra of LTO electrodes after formation and ageing with the Base electrolyte, Base + 1.0 wt % LiBOB, Base + 2.0 wt % LiBOB, Base + 1.0 wt % DFOB, and Base + 1.0 wt % TMSB.

Figure 3.5

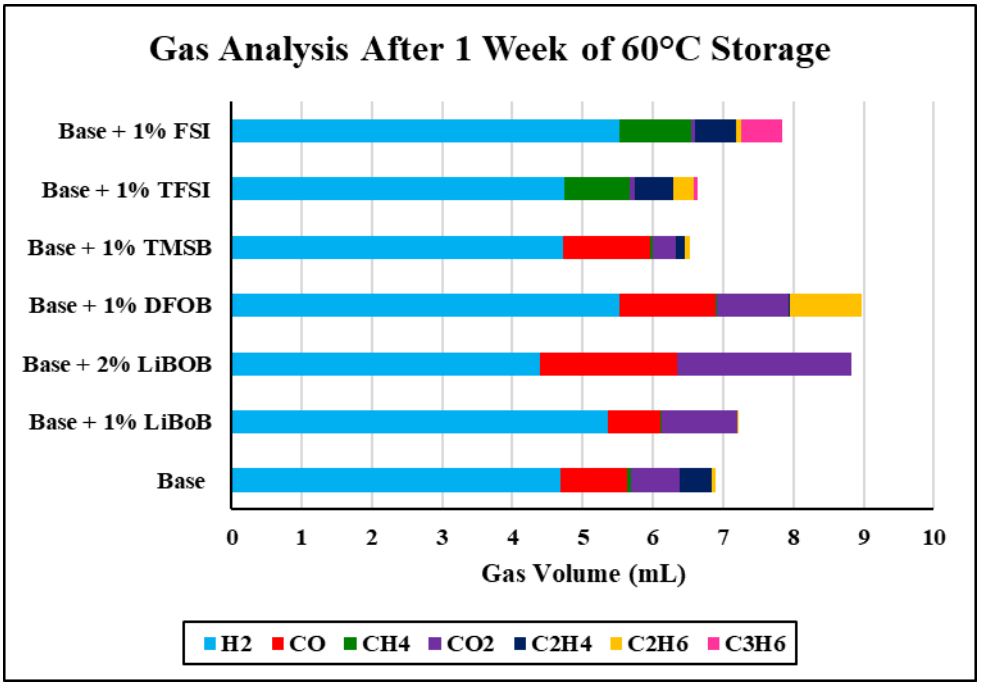

Figure 3.5 - Average volume of gas (left) and composition of gas generated after formation, ageing, and 1 week of storage at 60 °C with the Base electrolyte, Base + 1.0 wt % TFSI, Base + 1.0 wt % FSI, Base + 1.0 wt % LiBOB, Base + 2.0 wt % LiBOB, Base + 1.0 wt % DFOB, and Base + 1.0 wt % TMSB

Figure 3.6

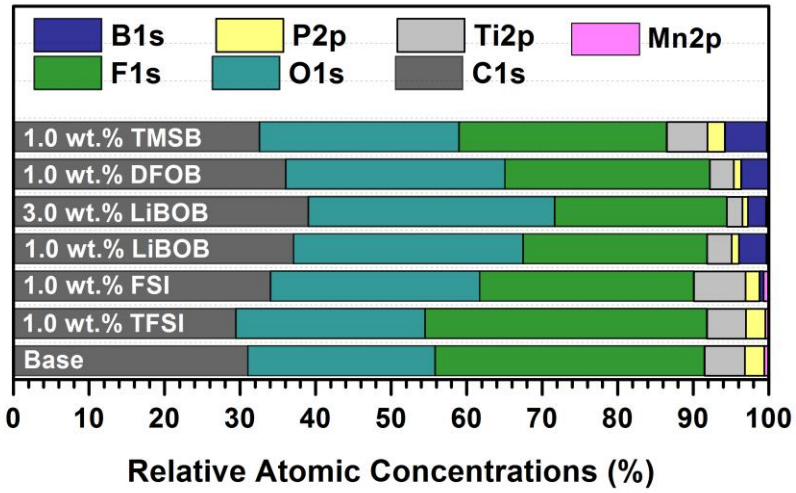

Figure 3.6 - Relative atomic concentrations of elements detected on the surface of LTO electrodes after formation, ageing, and 1 week of storage at 60 °C with the Base electrolyte, Base + 1.0 wt % TFSI, Base + 1.0 wt % FSI, Base + 1.0 wt % LiBOB, Base + 3.0 wt % LiBOB, Base + 1.0 wt % DFOB, and Base + 1.0 wt % TMSB.

Figure 3.7

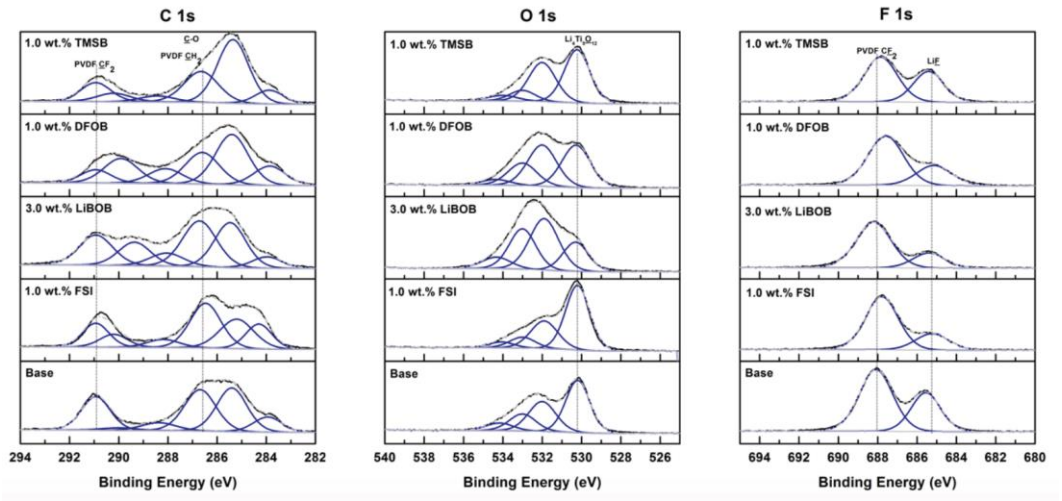

Figure 3.7 - C 1s, O 1s, and F 1s core spectra of LTO electrodes after formation, ageing, and 1 week of storage at 60 °C with the Base electrolyte, Base + 1.0 wt % FSI, Base + 3.0 wt % LiBOB, Base + 1.0 wt % DFOB, and Base + 1.0 wt % TMSB

Figure 3.8

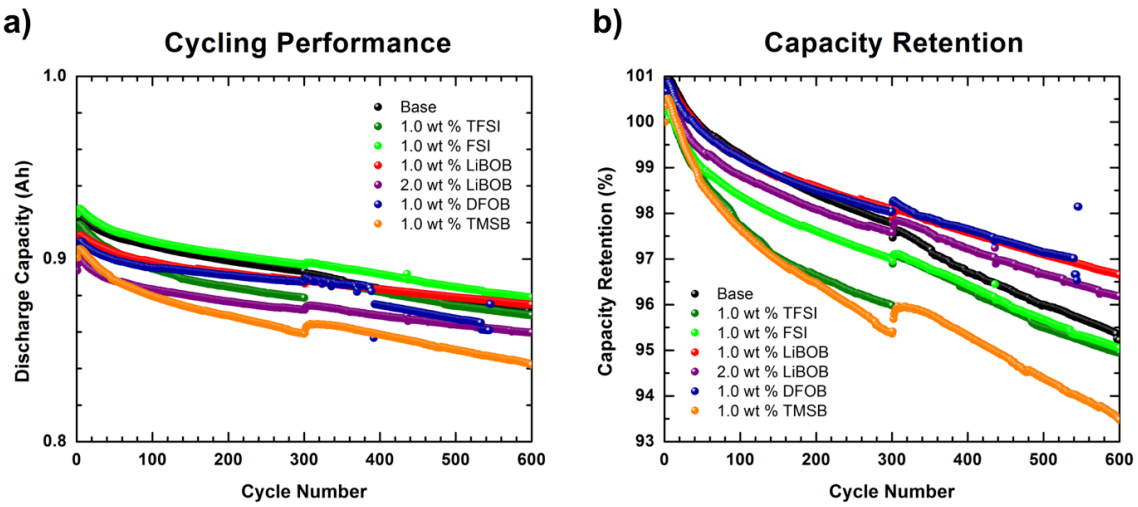

Figure 3.8 - Cycling performance (a) capacity retention (b) of long term cycling at 45 °C with the Base electrolyte, Base + 1.0 wt % TFSI, Base + 1.0 wt % FSI, Base + 1.0 wt % LiBOB, Base + 2.0 wt % LiBOB, Base + 1.0 wt % DFOB, and Base + 1.0 wt % TMSB.

Figure 3.9

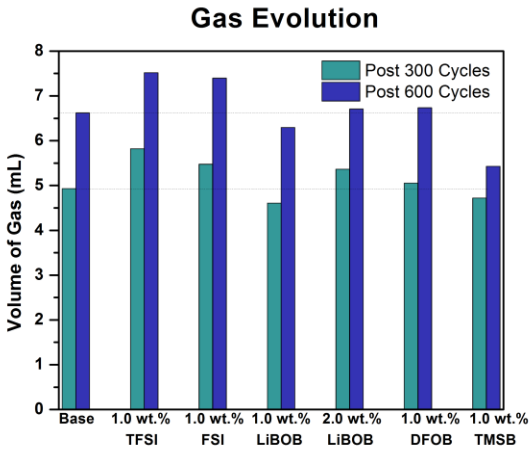

Figure 3.9 - Volume of gas generated after 300 and 600 cycles at 45 °C with the Base electrolyte, Base + 1.0 wt % TFSI, Base + 1.0 wt % FSI, Base + 1.0 wt % LiBOB, Base + 2.0 wt % LiBOB, Base + 1.0 wt % DFOB, and Base + 1.0 wt % TMSB.

CHAPTER 4

THE EFFECTS OF TRIS(TRIMETHYLSILYL)PHOSPHATE AND PHOSPHAZENE ADDITIVES ON $LiNi_{0.8}Co_{0.1}Mn_{0.1}O_2$ DURING HIGH TEMPERATURE CYCLING

By

Jennifer Hoffmann[1,2], Martin Payne[2], Brett Lucht[3]

Manuscript Pending Publication in Journal of Electrochemistry

[1]PhD candidate, Department of Chemistry, The University of Rhode Island, Kingston, RI 02882.

[2]Battery R&D, Gotion Inc., Independence, Ohio 44131, USA

[3]Professor, Department of Chemistry, The University of Rhode Island, Kingston, RI, 02882.

Abstract

Lithium ion batteries are the most competitive technology to be adopted by the growing electric vehicle industry. With that comes growing demands for materials that deliver higher capacity. One cathode material that stands out due to its ability to supply high capacity is $LiNi_{0.8}Co_{0.1}Mn_{0.1}O_2$ (NCM811). This material comes with safety and cycle life issues due to the side reactions commonly leading to harmful phase changes, active material absorption, and cationic mixing. Researchers have primarily used different coating and synthesis techniques in attempts to stabilize the cathode material. This work focuses on using tris(trimethylsilyl)phosphate (TMSP) and Ethoxy pentafluoro cyclotriphosphazene (PFPN) to improve the long term, high temperature performance and safety of the system. Through electrochemical measurements, gas analysis, and impedance spectroscopy, TMSP was proven to have performance benefits for the material reaching 78% capacity retention after 200 cycles at 60°C. TMSP also showed to reduce impedance after long term, high temperature cycling.

Introduction

With today's market transitioning to hybrid electric vehicles (HEVs) and electric vehicles (EVs), the demand for lithium ion batteries is ever increasing. In order to meet the requirements of an HEV or EV lithium ion battery, the battery must have high energy density, long cycle life, a wide operating temperature range, and be safe. In order to meet this criterion, advanced materials such as high nickel cathode materials are explored. One high nickel cathode material that has the attention of many researchers today is $LiNi_{0.8}Co_{0.1}Mn_{0.1}O_2$ (NCM811) due to its high capacity capabilities.[1] This material combines the beneficial rate capabilities of cobalt, while keeping the material at a more price conscious level, with the high capacity capabilities of nickel and life cycle of manganese.[2-3]

Although it seemingly is an all-encompassing material, NCM811 has many issues that come as trade-offs. The high amount of nickel content that leads to the increased capacity is also thermally unstable. As the Ni^{2+} has a similar ionic radius to Li^+, cationic mixing occurs and the resulting Ni^{4+} that is predominant at the end of charge leads to undesired side reactions that decreases safety and cycle life while increasing gassing, active material consumption, and inactive phase changes.[1,2,5] To combat this, researchers have been focusing on different coating and preparation techniques to stabilize the nickel including surface modification with fluorine substitution[7], metallic ion doping[8-11], spherical hydroxide precursor with Li_3PO_4 coating[6], and coating thinner electrodes[12]. In this work, we focused on the electrolyte as a solution by testing various additives with SEI or gas reducing properties. The additive tris(trimethylsilyl)phosphate has been reported to show benefits under room

temperature for high voltage NCM systems by forming and SEI on the cathode.[13,14] This additive was selected for this reason as well as reports that other tris(trimethylsilyl) additives have also stabilized the graphite anode. Ethoxy pentafluoro cyclotriphosphazene (PFPN) was also selected for its known safety benefits.[17,18] Using these two concepts, this work examines if the electrolyte can improve the use of NCM811 as an advanced cathode material.

Experimental

Materials

Battery grade ethylene carbonate (EC), propylene carbonate (PC), dimethyl carbonate (DMC), ethyl methyl carbonate (EMC), lithium hexafluorophosphate ($LiPF_6$), were provided by Gotion and used as received. Battery grade 1,3-Propane Sultone (PS) and vinyl carbonate (VC), and Ethoxy pentafluoro cyclotriphosphazene (PFPN) were obtained from BASF and used as received. Battery grade tris(trimethylsilyl)phosphate (TMSP) was purchased from Sigma Aldrich and used as received. The base electrolyte formulation, B66, consisted of 1.0 M LiPF6 in EC/PC/DMC/EMC (25/10/25/40, wt) + 2% VC + 1% PS. B44 formulation is the baseline + 1% PFPN. B45 formulation is the baseline + 1% PFPN and 1%TMSP. B50 formulation is the baseline + 1%TMSP.

Cell Preparation

Pouch cells – 460 mAh multilayer pouch cells were assembled by SKC using commercially available $LiNi_{0.8}Co_{0.1}Mn_{0.1}O_2$ (NCM811) as the cathode material and commercially available graphite anode material. The cells were dried at 55 °C for 12 hours under vacuum prior to filling. Once dried, cells were transferred to an argon glove box and filled with 2.45 g of electrolyte and vacuum sealed. All cells undergo 12 hours of rest at 25 °C after sealing to ensure complete wetting. Electrochemical data and gas measurements were obtained from pouch cells.

Electrochemical Testing

Formation and Aging – Pouch cells were clamped and cycled with a constant current (CC) charge at 0.1C with a 3.7 V cutoff voltage using a MACCOR battery cycler. Once charged, the cells were unclamped and placed in a 45 °C chamber for 12 hours of aging. Cells were then degassed and vacuum-sealed in the argon glove box before undergoing a second formation step in which the cells were cycled with a constant current-constant voltage (CC-CV) charge and CC discharge between 4.2 and 2.8 V with the following procedure: 1 cycle at C/10, 1 cycle at C/5, and 1 cycle at 1C.

Long Term Cycling – After completing the formation and aging procedure, cells undergo rate testing between 4.2 and 2.8 V according to the following procedure: 2 cycles with C/2, D/2; 1 cycle with C/2, D/5; 1 cycle with C/2, D/2; 1 cycle with C/2, 1D; 1 cycle with C/2, 2D; and 3 cycles with C/2, D/2 (where C = charge rate and D = discharge rate). Once the rate testing is complete, volume and impedance measurements were taken as referenced in the respective experimental descriptions. Upon completion, cells were transferred to a 60 °C chamber (tightly clamped) and

cycled between 4.2 and 2.8 V at 1C for 200 cycles with the AC and DC impedance measured after each charging step of each cycle.

All cells were prepared in duplicates to confirm reproducibility. Representative data is presented.

Gas Analysis

Gas Volume – Gas volume was measured before first formation and after aging before degassing according to the procedure first described by Aiken et al. The pouch cells were hung from the bottom of scale and tarred. After reaching a stable zero, the cells were submerged completely to a defined level in 25°C deionized water. The recorded weight of the cell while submersed was then used along with the Archimedes' principle to calculate the amount of gas evolved over time[11].

Gas Composition – To measure the composition of gasses, cells were brought into the argon dry box for extraction. A 0.5 mL Vici precision sampling analytical pressure-lok syringe was used to manually extract the gas sample from the cell under argon atmosphere. The sample was then manually injected into a Varian 450 gas chromatograph equipped with a 19808 ShinCarbon ST column, thermal conductivity detector (TCD), and an argon carrier gas.

Impedance

Electrochemical Impedance Spectroscopy (EIS) – EIS was measured on all pouch cells before and after high temperature cycling in the discharged state. All

measurements were taken at 25°C with a Solartron Analytical modulab 2100A potentiostat with a 5 mv amplitude with the frequency sweep between 1000 kHZ – 25 mHz.

Results and Discussion

The results from cycling for 200 cycles at 60°C can be seen in Figure 4.2 where the capacity in Ah and the capacity retention (%) is compared. The formulation containing TMSP (B50) outperformed the baseline and other formulations tested by having 78.2% capacity retained, which was about an 8% improvement over the baseline. The baseline, B66, displayed a capacity retention of about 70%. While the formulation containing PFPN did start off with an improved capacity over the baseline, around 120 cycles the fading increased to result in about 66% capacity retention after 200 cycles. The worst performing formulation was the combination of the two additives explored in this work with only 60% capacity remaining after 200 cycles.

Looking into explanations as to why this occurred, the AC impedance data presented in Figure 4.3 shows B50 with the lowest impedance increase throughout cycling despite the second highest initial impedance. The formulations containing TMSP, B45 and B50, show similar impedance until about 100 cycles. After 100 cycles, B45 increases in impedance rapidly, while B50 does not increase in this way. Formulations B66, B44, and B45 all have very similar impedance at the end, indicating TMSP is helping the impedance of the cell while PFPN may be not be as beneficial for the impedance. The EIS data in Figure 4.4 gives another look into the impedance trends seen during cycling. B44 shows the largest total impedance before

cycling with B45 and B50 having very similar performance again. After cycling, B50 has significantly lower impedance than the other formulations including the baseline indicating the impedance benefits of TMSP. B44 and B45 show similar performance higher than B50 but lower than B66 which is showing the highest impedance of all formulations.

Due to the performance and impedance data, the differential capacity for the first formation is referenced to determine any possible changes between the additive formulations. As Figure 4.5 shows, the formulations containing TMSP display peak changes around 2.38V, 2.7V and 2.85V respectively. At 2.38V, B45 and B50 show a slight shift in the baseline peak. B44 does not show this shift. This is an early indication that TMSP is protecting the formation of or forming a different SEI. To further confirm this, B50 shows the strongest increase in intensity of the peak at 2.7V. Formulation B45 shows a similar increase, although not as intense. The baseline and PFPN formulation do not show a difference at this peak and remain similar. TMSP formulations also shows a peak at 2.85V which is not present in the baseline or B44. TMSP formulations also show a leveling of a small peak seen in B66 and B44 around 2.19V.

Formation gas analysis shows that TMSP containing formulations had the largest amount of formation gasses present as seen in Figure 4.6. While B44 did show a decrease in the formation gassing, the gas composition does not vary significantly from B66. The formation gas produced by the baseline was primarily ethylene and methane at just under 34% each. Figure 4.7 shows that the largest change in formation gas composition was with B50 reducing the amount of ethylene by 8% and the

hydrogen gas by almost 2%. This gas reduction was accompanied by an increased in the carbon monoxide produced. TMSP may have stabilized the solvent interactions through SEI formation but forming that SEI releases increased levels of carbon monoxide.

Conclusions

The electrolyte additive TMSP improves the cycling capacity at 60°C while reducing the impedance of the system. TMSP likely does this through SEI formation that stabilizes the electrolyte based on differential capacity and formation gas analysis data. During the SEI formation process, an increased level of gas is produced as a side product. While the main gasses produced in the NCM811/C system are methane, ethylene, and carbon monoxide, TMSP reduces the ethylene and increases the carbon monoxide. This SEI formation and formation mechanism will be confirmed with X-ray photoelectron spectroscopy (XPS) surface analysis. The phosphazene additive, PFPN, showed no added benefits to the system. To the contrary, PFPN hurt the cell capacity performance with little improvement to the impedance and formation gas evolution.

References

1. Ding, Y.; Mu, D.; Wu, B.; Wang, R.; Zhao, Z.; Wu, F., Recent progress on nickel rich layered oxide positive electrode materials used in lithium-ion batteries for electric vehicles. *Applied Energy* **2017,** *195,* 586-599.

2. Wang, L.; Li, J.; He, X.; Pu, W.; Wan, C.; Jiang, C., Recent advances in layered $LiNi_xCo_yMn_{1-x-y}O_2$ cathode materials for lithium ion batteries. *J. Solid State Electrochem* **2009,** *13,* 1157-1164.

3. Noh, H.; Youn, S.; Yoon, C.S.; Sun, Y., Comparison of the structural and electrochemical properties of layered $Li[Ni_xCo_yMn_z]O_2$ (x=1/3, 0.5, 0.6, 0.7, 0.8 and 0.85) cathode material for lithium-ion batteries. *Journal of Power Sources,* **2013,** *233,* 121-130.

4. Manthiram, A.; Song, B.; Li, W., A perspective on nickel-rich layered oxide cathodes for lithium-ion batteries. *Energy Storage Materials,* **2017,** 125-139.

5. Schipper, F.; Erickson, E.; Erk, C.; Shin, J.; Chesneau, F., Aurbach, D., Review -Recent advances and remaining challenges for lithium ion battery cathodes. *Journal of the Electrochemical Society*, **2017,** *164* (1), A6220-A6228.

6. Wang, M.; Zhang, R.; Gong, Y.; Su, Y.; Chen, L.; Chen, Y.; Luo, M. ; Chu, M., Improved electrochemical performance of the $LiNi_{0.8}Co_{0.1}Mn_{0.1}O_2$ material with lithium-ion conductor coating for lithium ion batteries. *Solid State Ionics.* **2017,** *312*, 53-60.

7. Woo, S.U.; Park, B.C.; Yoon, C.S.; Myung, S.T.; Prakash, J.; Sun, Y.K., Improvement of Electrochemical performances of $Li[Ni_{0.8}Co_{0.1}Mn_{0.1}]O_2$ cathode

materials by Fluorine substitution. *Journal of the Electrochemical Society*, **2007,** *154* (7), A649-A655.

8. Park, B.C.; Kim, H.B.; Myung, S.T.; Amine, K.; Belharouak, I.; Lee, S.M.; Sun, Y.K., Improvement of structural and electrochemical properties on AlF_3-coated $Li[Ni_{1/3}Co_{1/3}Mn_{1/3}]O_2$ cathode materials on high voltage region. *Journal of Power Sources* **2008,** *178,* 826-831.

9. Xiong, X.H.; Wang, Z.X.; Guo, H.J.; Zhang, Q.; Li, X.H., Enhanced electrochemical properties of lithium-reactive V_2O_5 coated on the $LiNi_{0.8}Co_{0.1}Mn_{0.1}O_2$ cathode material for lithium batteries at 60°C¸ *Journal of Materials Chemistry* **2013,** 1284-1288.

10. Woo, S.W.; Myung, S.T.; Bang, H.; Kim, D.W.; Sun, Y.K., Improvement of electrochemical and thermal properties of $LiNi_{0.8}Co_{0.1}Mn_{0.1}O_2$ positive electrode materials by multiple metal (AL, Mg) substitution. *Electrochimia Acta* **2009,** *54*, 3851-3856.

11. Wu, F.; Wang, M.; Su, Y.F.; Bao, L.Y., Chen, S., A novel layered material of $LiNi_{0.32}Co_{0.33}Mn_{0.33}Al_{0.01}O2$ for advanced lithium-ion batteries. *Journal of Power Sources* **2010,** *195*, 2900-2904.

12. Liu, S.; Xiong, L.; He, C., Long cycle life lithium ion battery with lithium nickel cobalt manganese oxide (NCM) cathode. *Journal of Power Sources* **2014,** *261*, 285-291.

13. Yan, G.; Li, X.; Wang, Z.; Guo, H.; Wang, C., Tris(trimethysilyl)phosphate: a film-forming additive for high voltage cathode material in lithium-ion batteries. *Journal of Power Sources* **2014,** *248*, 1306-1311.

14. Liao, X.; Zheng, X.; Chen, J.; Huang, Z.; Xu, M.; Xing, L.; Liao, Y.; Lu, Q.; Li, X.; Li, W., Tris(trimethylsilyl)phosphate as electrolyte additive for self-discharge suppression of layered nickel cobalt manganese oxide. *Electrochemicia Acta*, **2016,** *212*, 352-359.

15. Mai, S.; Xu, M.; Liao, X. ; Hu, J. ; Lin, H. ; Xing, L. ; Liao, Y. ; Li., X. ; Li, W., Tris(trimethylsilyl)phosphite as electrolyte additive for high voltage layered lithium nickel cobalt manganese oxide cathode of lithium ion battery. *Electrochemicia Acta*, **2014,** *147*, 565-571.

16. Qi, X.; Tao, L.; Hahn, H.; Schultz, C.; Gallus, D.R.; Cao, X.; Nowak, S.; Röser, S.; Li, J.; Cekis-Laskovic, I.; Rad, B.R.; Winter, M.; Lifetime limit of tris(trimethylsilyl)phosphite as electrolyte additive for high voltage lithium ion batteries. *RCS Adv.* **2016**, *6*, 38342-3849.

17. Li, X.; Li, W.; Chen, L. ; Lu, Y. ; Su, Y. ; Bao, L. ; Wang, J. ; Chen, R. ; Chen, S. ; Wu, F. , Ethoxy(pentafluoro) cyclotriphosphazene (PFPN) as a multi-functional flame retardant electrolyte additive for lithium-ion batteries. *Journal of Power Sources* **2018,** *378*, 707-716.

18. Xia, L.; Xia, Y.; Liu, Z., A novel fluorocyclophosphazene as bifunctional additive for safer lithium-ion batteries. *Journal of Power Sources* **2015,** *278*, 190-196.

Figure 4.1

a.

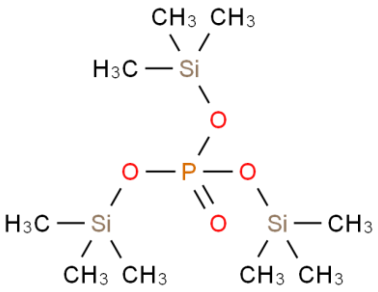

b.

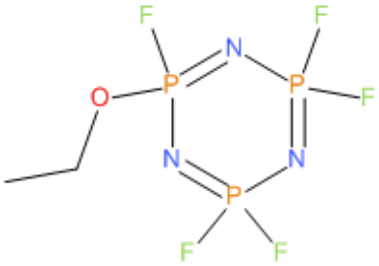

Figure 4.1 – Chemical structures of TMSP and PFPN additives

Figure 4.2

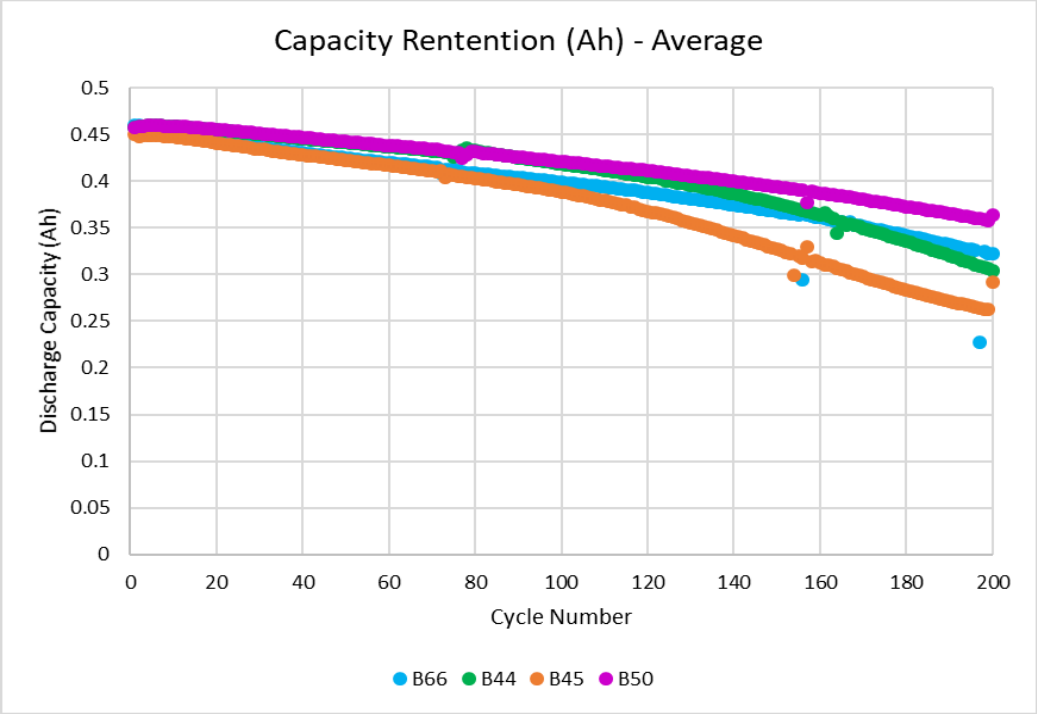

Figure 4.2- Discharge capacity for formulations undergoing cycling in 60°C for the baseline (B66), base + 1% PFPN (B44), base + 1%PFPN + 1%TMSP (B45), and base + 1%TMSP (B50). Formulation B50 showed 78% capacity retention after 200 cycles.

Figure 4.3

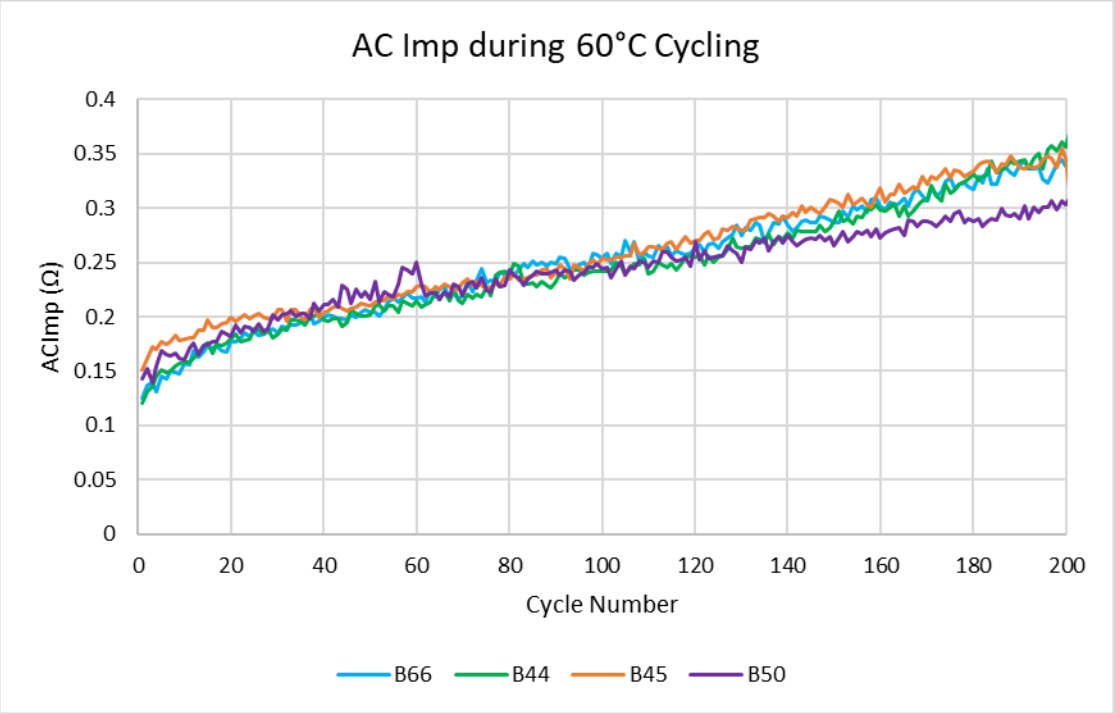

Figure 4.3- AC impedance during 60°C cycling measured during 100% state of charge for all formulations. AC impedance measurement was performed by the MACCOR battery cycler.

Figure 4.4

a.

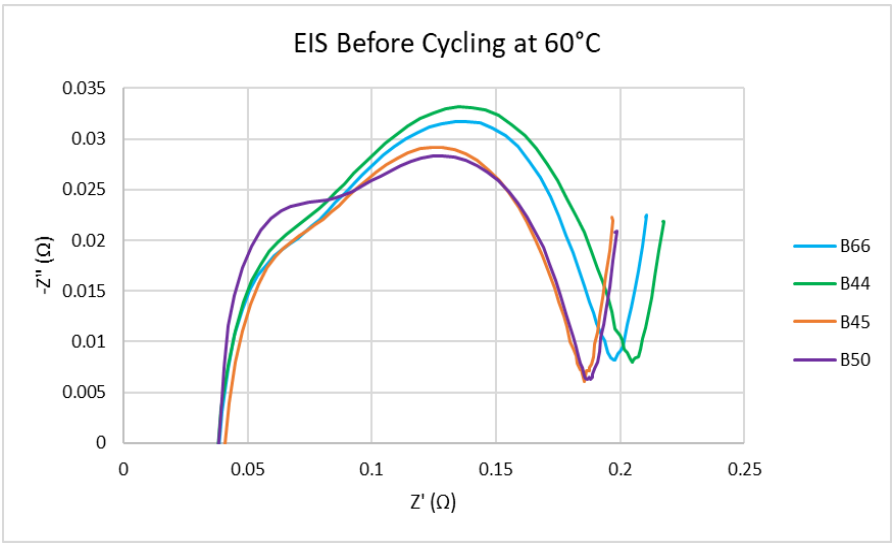

b.

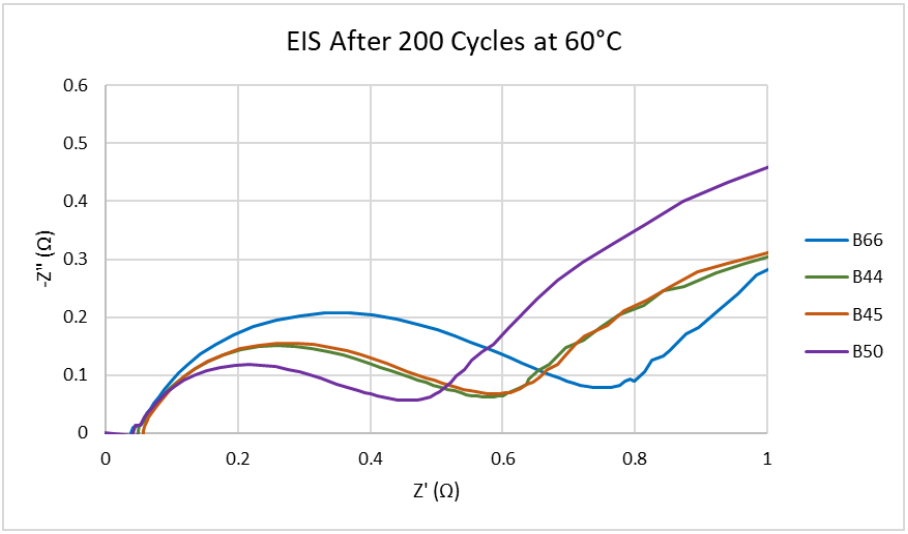

Figure 4.4- EIS impedance spectra for a. before and b. after 60°C cycling. EIS for the after cycling test was taken after 200 cycles.

Figure 4.5

a.

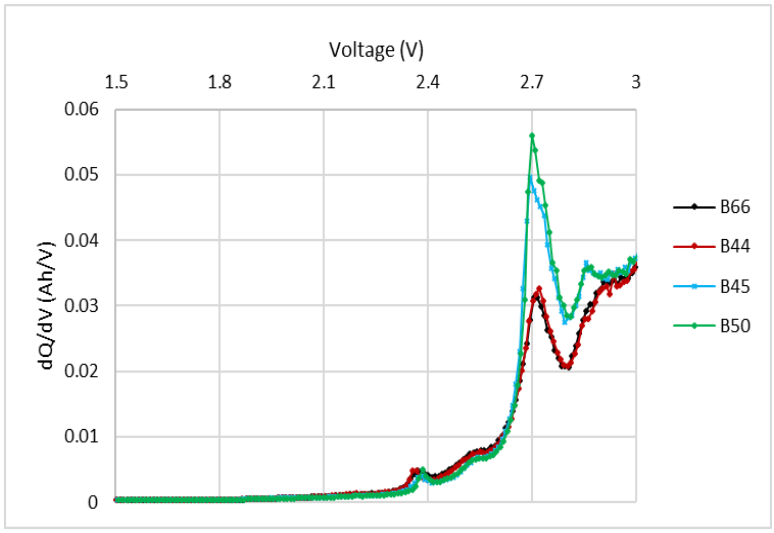

b.

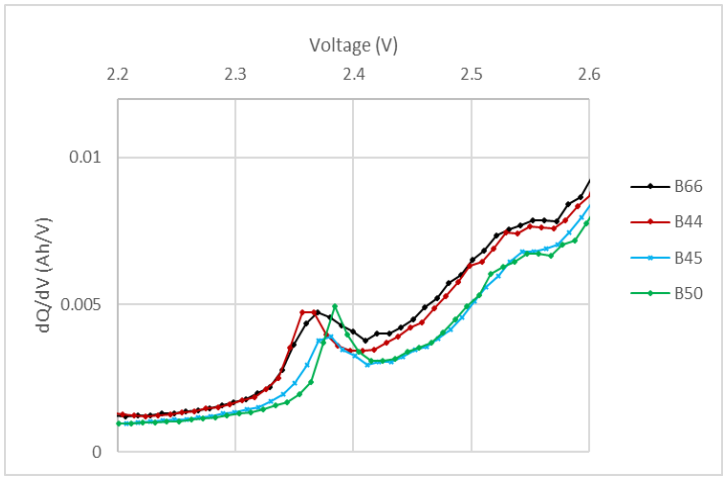

Figure 4.5- Data from the first formation charge before aging was used to look at the dQ/dV for each formulation. Plot a. shows the charge in its entirey with b. showing a closer look at the lower voltage curve differences.

Figure 4.6

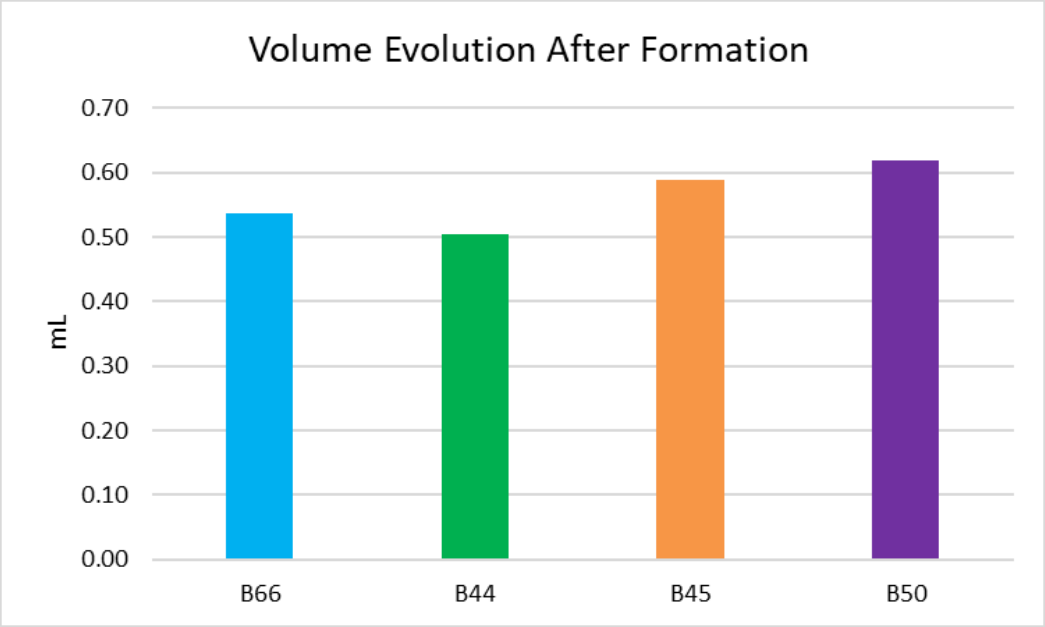

Figure 4.6 – Volume data was acquired to determine the gas evolution after formation and aging at 45°C for 12 hours.

Figure 4.7

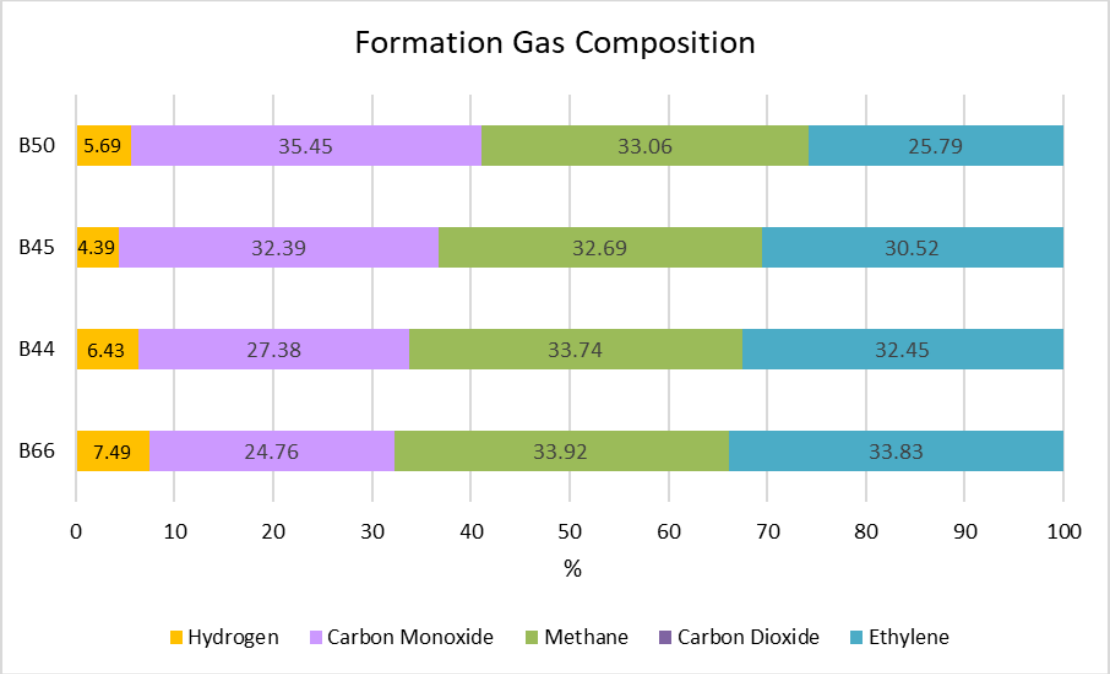

Figure 4.7 – The gas composition presented as a percent for each formulation after undergoing formation and 45°C aging for 12 hours.